Diamond & Related Materials 153 (2025) 112039

Contents lists available at ScienceDirect

Diamond & Related Materials

journal homepage: www.elsevier.com/locate/diamond

A scaffold material: Reduced graphene oxide and carbon quantum dots filled polycaprolactone nanofibers

Ferda Mindivan *, Büşra Boz

Department of Bioengineering, Bilecik Seyh Edebali University, Bilecik, Turkey

ARTICLE INFO

Keywords:
Reduced graphene oxide
Carbon quantum dots
Polycaprolactone
Electrospinning
Nanofibers
Tissue scaffold materials

ABSTRACT

In this study, a comparative analysis was conducted between the properties of poly(ε-caprolactone) (PCL)-based electrospun nanofibers filled with both reduced graphene oxide (RGO) and carbon quantum dots (CQDs). Both RGO and CQD fillers interacted with PCL, modifying the crystal structure and enhancing thermal stability. The addition of RGO increased the nanofiber diameter, whereas the inclusion of CQDs reduced it. The incorporation of CQDs resulted in a significant increase of up to 73 % in the elastic modulus, while RGO led to a smaller increase of only 1.9 %. CQDs also contributed to a 160 % increase in nanoscale hardness, while RGO caused a maximum increase of 40 %. Furthermore, CQDs enhanced the storage modulus by 210.79 % and the loss modulus by 595.27 %. In terms of biodegradability, CQDs, with lower contact angles (72.29° - 68.75°), degraded more than the nanofibers containing RGO (74.96° - 70.15°), showing similar biodegradability. The bioactivity test results indicated that both RGO and CQD fillers promoted the formation of apatite; however, neither exhibited antibacterial activity. This study suggests that CQDs are a more advantageous filler compared to RGO, based on their greater impact on the structural, thermal, mechanical, and biological properties of PCL.

1. Introduction

Every year, bone tissue damage leads to surgical operations and tissue transplants around the world. Scaffolds are used to recreate the extracellular matrix damaged by disease, injury, or congenital defects, as well as provide support to cells [1]. Electrospinning is known as an excellent technique for producing tissue scaffolds. This technique is used to produce micro- and nanofibers from natural or synthetic polymers to obtain scaffolds with high surface area and porosity [2]. Compared to other nanofiber production methods, its high performance, affordability, and ease of use make it preferred [3]. A synthetic aliphatic polyester that is both biocompatible and biodegradable, polycaprolactone (PCL) is one of the most widely used biopolymers in the production of electrospun nanofibers. Furthermore, PCL is characterized by its straightforward manufacturing process, user-friendly nature, affordable price [4] and important mechanical properties [5]. The hydrophobic structure of PCL, its slower degradation rate compared to other polymers, lack of bioactivity, and absence of antibacterial properties prevent it from possessing the features of a tissue scaffold. Researchers aim to improve the disadvantages properties of PCL by blending it with various polymers or including different additives into the PCL matrix. This approach is used to create tissue scaffolds with certain desired characteristics [5,6]. Researchers have recently incorporated graphene derivatives into the PCL matrix to disrupt the hydrophobic nature of PCL, enhance its solubility in solutions, provide antibacterial properties, and reduce the degradation time [7]. Better cell adhesion and proliferation characteristics, excellent mechanical strength, and a regulated rate of degradation are all present in PCL/graphene nanofibers. This is because their interaction, physicochemical characteristics, and biocompatibility all combine to strengthen them [8]. In this study, reduced graphene oxide (RGO) was used as one of the graphene derivatives. RGO, one of the graphene derivatives with oxygen-containing groups, is widely used as a potential additive to improve the chemical and physical properties of PCL-based composites due to its excellent properties, such as high thermal conductivity, high elastic modulus, high strength, and large specific surface area [9]. Zero-dimensional carbon quantum dots (CQDs), which are increasingly popular among carbon-derived fillers, are a hemispherical carbon allotrope. They have been the focus of many studies because of their properties, such as exceptional solubility, easy functionalization, chemical stability, and low toxicity compared to one-dimensional carbon nanostructures. CQDs have many application areas, such as

* Corresponding author.
E-mail address: ferda.mindivan@bilecik.edu.tr (F. Mindivan).

https://doi.org/10.1016/j.diamond.2025.112039
Received 5 December 2024; Received in revised form 12 January 2025; Accepted 26 January 2025
Available online 27 January 2025

biosensors, drug delivery systems, optoelectronics, white light-emitting diodes, and solar cells [10,11]. The homogeneous distribution of nano-sized CQDs in polymer matrices has resulted in significant improvements in the physical and chemical properties of tissue scaffolds produced by electrospinning [12]. In this study, the electrospinning method was used to produce nanofibers with improved thermal and mechanical properties by adding micro-sized RGO and nano-sized CQDs to the PCL matrix. Table 1 summarizes the most recent literature studies on the application of nanofibers produced through electrospinning polymer composites and nanocomposite solutions incorporating graphene derivatives and CQDs additives inside the PCL matrix for tissue scaffolds. In the literature review, the morphological, mechanical, thermal, electrical, and biological test results of nanofibers produced by adding graphene derivatives and CQDs to the PCL matrix showed that graphene derivatives and CQDs are effective in providing the desired properties of a tissue scaffold. The number of studies with GO is particularly large. The literature review identified two studies using RGO. Ishwarchand et al. [9] and Gohari et al. [12] produced the RGO chemically with hydrazine hydrate and vitamin C, respectively. The methanol extraction of rosehip fruit provided the RGO for this article [18]. Nanofiber studies produced by adding CQDs to the PCL matrix are also quite limited and very new. Additionally, the hydrothermal method [19] produced the CQDs from rosehip fruit used in this study. Therefore, there is no study in the literature regarding both RGO and CQDs additives produced from rosehip fruit added to the PCL matrix to obtain nanofibers. There is no study in the literature that compares the two additives. Therefore, this study is the only and original study using RGO and CQDs fillers produced by green synthesis.

2. Materials and methods

2.1. Materials

Poly(ε-caprolactone) (PCL, Mn = 80,000, Code:178305000) was supplied by Acros Organics. RGO [18] and CQDs [19] used as fillers in this study were obtained from our previous studies. Dimethyl formamide (99.9 %, DMF, UN 2265) and chloroform (99.9 %, CL, UN 1888) solvents were purchased from Carlo Erba Reagents. Phosphate buffered saline (PBS, pH = 7,4 (1×), REF: 10010-015) was supplied by GIBCO (USA). Simultene Body Fluid (SBF) was purchased from Biochemazone. Mueller-Hinton, Agar SPC, *E. coli* ATCC 25922, and *S. aureus* ATCC 25923 were obtained from ATCC, USA.

2.2. Preparation of PCL, PCL/RGO and PCL/CQDs electrospun solution

To prepare polymer solutions with a concentration of 15 wt%, PCL was dissolved in the mixtures of DMF and CL (1:4 *v*/v) and stirred at a constant rate for 3 h at room temperature. Next, RGO and CQDs were added to the solution at aspect ratios of 0.5;1.0;1.5; 2.0, and 5.0 wt% and stirred to achieve a homogenous solution. The mixture was stirred for 30 min for the 0.5 wt% addition and 60 min for the 1.0 wt% addition, based on the wt% values of the fillers, respectively. The wt% value was calculated by weighing RGO, which was solid. The liquid drying method determined the concentration of CQDs, which were liquid [20]. The contents of the polymer solutions prepared for nanofiber production and nanofiber codes were given in Table 2.

2.3. Fabricating electrospun PCL, PCL/RGO and PCL/CQDs nanofibers

Scaffold structures produced by electrospinning are notable for their high surface-to-volume ratio and mechanical strength, which closely mimic the extracellular matrix (ECM) [14]. The prepared solutions were transferred into a 10-mL syringe with a blunt-end needle of 19 gauges. The solution was pumped out of the syringe at a rate of 1.5 mL/h, and a high voltage of 10 KV was applied for electrospinning. The electrospinning distance, from needle tip to collector, was 12 cm. The rotary

Table 1
Nanofiber studies produced by the electrospinning method with the addition of graphene derivatives and CQDs fillers to the PCL matrix for tissue engineering applications.

Authors	Year	Fillers for PCL nanofibers	Results
Karapehlivan et al. [13]	2024	Graphene oxide (GO) and collagen (COL)	A high amount (3 % and 5 %) of COL decreased the tensile strength, while COL addition increased cell viability. The direct current (DC) conductivity values ranged from 1.10×10^{-10} to 6.10×10^{-10} S/m at 25 °C. The alternating current (AC) conductivity values exhibited frequency-dependent behavior.
Loyo et al. [14]	2023	Graphene oxide GO and gelatin (Gt).	The incorporation of 1 wt% and 2 wt% GO into PCL resulted in a significant reduction in fiber diameter by 23.2 % and 28.8 %, respectively, compared to neat PCL fibers.
Ishwarchand et al. [9]	2022	Reduced graphene oxide (RGO)	The diameters ranged from 107 nm to 226 nm, and the microstrain values varied from 0.00243 to 0.0043. RGO did not affect the crystal structure.
Rastegar et al. [15]	2021	Polyglycerol sebacate (PGS) and CQDs	The average nanofiber diameters of PGS/PCL and PGS/PCL/CQDs were 862 ± 167 nm and 376.82 ± 150 nm, respectively. CQDs increased electrical conductivity but decreased cell viability. The elastic modulus, elongation at break, and tensile strength of the PGS/PCL/CQDs (2:1:0.5) nanofiber were 11 ± 1 MPa, 10 ± 1 mm, and 5 ± 1 MPa, respectively.
Gohari et al. [12].	2021	Reduced graphene oxide (RGO)	RGO increased the fiber diameter, degradation rate, surface roughness, cell viability, and alkaline phosphatase activity in the PCL scaffold containing 1.0 wt% RGO compared to pure PCL ($P < 0.05$).
Ghorghi et al. [5]	2020	CQDs and captopril (CP)	The addition of CQDs and CP decreased the fiber diameter from 1180 ± 281.5 nm to 345 ± 110 nm, increased surface hydrophilicity (from 137° to 0°), and enhanced cell proliferation and ALP activity. The ultimate tensile strength of the scaffolds ranged from 6.86 ± 0.00 MPa to 22.09 ± 0.06 MPa.
Faraji et al. [7]	2020	Graphene oxide (GO) and quercetin (Q)	GO nanosheets and GO/Q composites reduced the fiber diameter while increasing cell viability to 95 %. The hydrophilicity decreased from 144° to 67°, and the addition of GO increased the tensile stress to 4 MPa.
Heidari et al. [16]	2017	Gelatin and GO	Gelatin increased the diameter of the nanofibers, whereas GO decreased it. The tensile strength and elastic modulus of the nanofibers increased significantly by 117 % and 128 %, respectively. Electrical conductivity was 11 times higher, and GO induced a more hydrophilic structure without showing any toxic effects on PC12 nerve cells. Additionally,

(*continued on next page*)

Table 1 (*continued*)

Authors	Year	Fillers for PCL nanofibers	Results
			GO enhanced the crystallinity of the material.
Ceretti et al. [17]	2017	Graphene nanoplatelet (GNP)	The addition of GNP increased the elongation value by 50 % and guided the differentiation of stem cells into a specific phenotype.
In this study,	2024	Reduced graphene oxide (RGO) and Carbon quantum dots (CQDs)	Max. polymer-filler interaction and max. crystallinity (8.2 %): **PCL/2CQDs** Max. crystal size and increasing interlayer distance: **PCL/1.5CQDs** Nanofiber diameter: **PCL/2RGO:265.24 nm and PCL/2CQDs:109.45 nm** Max. elastic modulus (73 %) and nanohardness (160 %): **PCL/1.5CQDs** Max. storage modulus (210.79 %) and loss modulus (595.27 %): **PCL/2CQDs** Contact angle: **PCL/2RGO:70.15° and PCL/2CQDs:68.75°** The highest % weight loss: **PCL/2RGO: 3.66 % and PCL/2CQDs: 3.75 %** Hydroxyapatite (Ca/P): **PCL/2RGO: 1.49 and PCL/2CQDs: 1.48** No antibacterial properties **PCL/CQDs** **PCL/RGO**

Table 2
The contents of the polymer solutions and nanofiber codes.

The codes of nanofiber	PCL wt%	RGO wt%	CQDs wt%
PCL	15	–	–
PCL/0.5RGO	15	0.5	–
PCL/1RGO	15	1.0	–
PCL/1.5RGO	15	1.5	–
PCL/2RGO	15	2.0	–
PCL/5RGO	15	5.0	–
PCL/0.5CQDs	15	–	0.5
PCL/1CQDs	15	–	1.0
PCL/1.5CQDs	15	–	1.5
PCL/2CQDs	15	–	2.0
PCL/5CQDs	15	–	5.0

drum's speed was 450 rpm. All the experimental procedures were done at 25 °C, and the moisture was %34–47. The nanofibers were subsequently vacuum dried to remove residual solvents. The most suitable electrospinning process parameters for the solutions during the preparation of nanofibers by electrospinning were determined by preliminary trials. In Fig. 1, photos showing the preparation of PCL polymer solutions and nanofibers, a sample microscope image of the fiber with the appropriate process parameter selected, and nanofiber samples prepared by the electrospinning method by selecting the most appropriate parameters were given.

2.4. Characterization techniques

2.4.1. Structural, thermal and electrical characterization

The interactions between the polymer and the fillers in all the

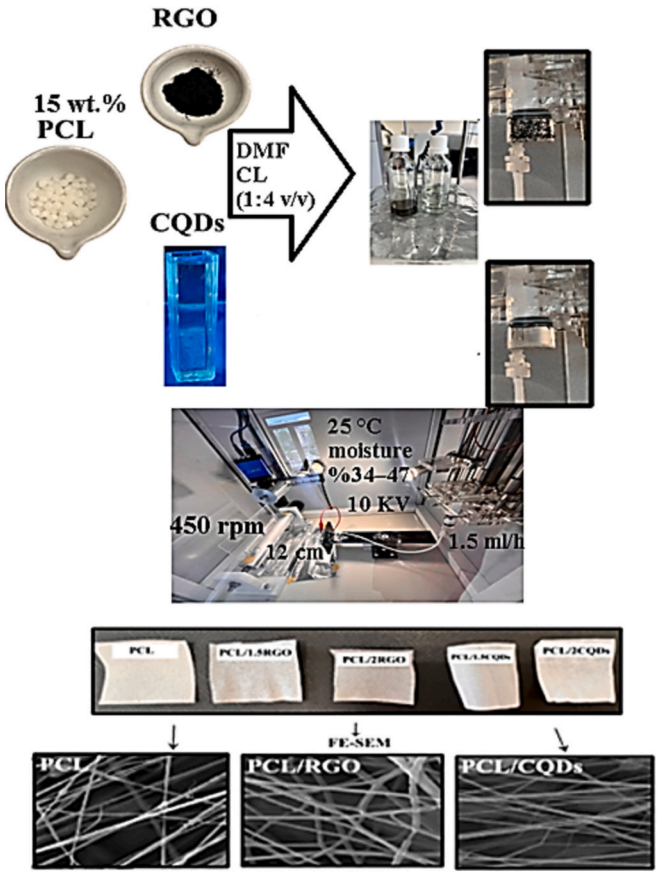

Fig. 1. Photos of the preparation of PCL polymer solutions and nanofibers.

nanofibers were observed on a Spectrum 100 Perkin Elmer model FTIR device in the wavenumber range of 400 and 4000 cm^{-1}. XRD analysis was performed to determine the crystal structures of PCL nanofibers with different filler additions and to show the formation of hydroxyapatite after the bioactivity test. The interlayer distance, crystallite size, and micro-strain values of the produced nanofibers corresponding to 2θ° were also taken from the XRD analysis results. XRD analyses of all nanofibers were performed at 2θ° = 5–30° angle range and 2°/min scanning speed. A Cu Kα (λ:1.5404) radiation PAN analytical Empyrean brand X-ray diffractometer was used. Thermal transitions were analyzed by Differential Scanning Calorimetry in a Setaram – Labsys Evo Instruments under nitrogen atmosphere, the thermal analysis was programmed at 10 °C/min from 25 to 200 °C, obtaining the melting temperature (Tm) and the melting enthalpy (ΔH_m). The degree of crystallinity (X_c %) was calculated using Eq. (1).

$$X_C = \frac{\Delta H_m}{\Delta H_m^0 (1 - w_{fibre})}.100 \quad (1)$$

Taking the value of crystallization enthalpy of pure crystalline PCL ΔH_m^0 as 139.5 J/g [14,21]. FE-SEM (Supra 40VP, Zeiss) analysis was performed to determine the nanofiber diameters, and observe the hydroxyapatite crystals formed on the nanofibers after the bioactivity test. Energy Dispersive Spectrometry (EDS) analysis together with FE-SEM was used to determine the Ca/P ratio, proving the formation of hydroxyapatite after the bioactivity test. Raman spectra and high-resolution images of the nanofiber samples were acquired using a confocal Raman microscope (Renishaw Invia Reflex) over a spectral range of 0–4000 cm^{-1}, equipped with a 532 nm wavelength laser. The resistances of each nanofiber were measured five times at room temperature using a standard four-probe Fytronix 9200 source meter brand electrical conductivity measuring device, and their conductivities were

calculated. The contact angles of the nanofibers were measured with the Fytronix 9000 Contact Angle Analyzer device.

2.4.2. Mechanical characterization

Nanoindentation tests of the PCL nanofibers were performed using the KLA+ Instruments iNano device at a constant strain rate (0.05 s^{-1}). The maximum penetration depth was selected as 500 nm. The sample was withdrawn while maintaining the same strain rate. It held the sample's load constant for 100 s. Dynamic mechanical analysis (DMA) was used to determine the mechanical properties of PCL nanofibers. DMA analysis of prepared samples with 10 mm length and 8 mm width were performed between −90 and 40 °C at a constant frequency of 1 Hz, a heating rate of 1.5 °C/min, and a loading rate of 0.1 N/mm using a preload of 0.05 N.

2.4.3. Biological characterization

Nanofibers were cut into rectangular shapes of 10 × 40 mm for biodegradation experiments. Their initial weights were recorded. They were kept in 10 mL of PBS solution at 37 °C and 100 rpm shaking speed in a water bath shaker for 56 days. Nanofibers were removed from the PBS solution on the 3rd, 7th, 14th, 21st, 28th, 42nd, 49th, and 56th days to determine their weight losses, washed with pure water, dried, and weighed. The weight losses of nanofibers were calculated according to Eq. (2). The initial weight (W_0) and the weight of the same sample after complete drying (W_d) were taken [22].

$$\text{Weight Loss}\ (\%) = \frac{W_0 - W_d}{W_0}.100 \quad (2)$$

It is known that biomaterials strengthen the tissue-biomaterial interface by releasing minerals such as Ca and P into the environment and providing natural biomineralization. In this study, the hydroxyapatite formation potential of nanofibers was obtained by immersing 1 × 1 cm^2 square samples in a 10 mL SBF solution [23]. Nanofiber samples immersed in SBF solution were removed from SBF at the end of the 1st and 7th days at 37 °C and dried. At the end of the first and seventh days, XRD and FE-SEM/EDS analysis showed that hydroxyapatite crystals had gathered on the nanofibers' surface. Previous studies determined that 7 days was sufficient for the formation of hydroxyapatite crystals, leading us to the limitation of 7 days for the bioactivity analysis [24]. Antibacterial tests of the PCL nanofibers were performed using a gram-negative bacterium (*Escherichia coli*) and a gram-positive bacterium (*Staphylococcus aureus*) using the disk diffusion analysis method. After streaking on Mueller Hinton Agar, it was incubated for 16–24 h at 37 °C. It was adjusted to a 0.5 McFarland standard (0.5 McFarland corresponds to 1–2108 bacteria). Bacteria were spread into different petri dishes for each bacterium with a sterile swab stick to cover the entire surface of the petri dishes. After the nanofibers were sterilized under bidirectional UV light for 1 h, they were placed in the petri dish and incubated at 37 °C for 16–24 h. After incubation, the zones formed by the sample were observed. The method was confirmed by the zone formation of the antibiotic used as a positive control (OXOID-5 μg disk).

3. Result and discussion

3.1. Structural, thermal and electrical analysis results

As shown in Fig. 2(a), the vibration bands of the functional groups of PCL were observed in the structure. It has been determined that the wavenumber values reported for PCL in the literature were consistent with the values obtained in this study [9,25–27]. The FTIR analysis results of PCL/RGO nanofibers shown in Fig. 2(b-c) at narrow range wavenumber values were compared with the wavenumber values of the pure PCL nanofiber. Shifts to lower wavenumber values were detected in the bands belonging to the asymmetric and symmetric stretching vibration of the -CH_2 group at wavenumbers of 2944.66 cm^{-1} and 2866.36 cm^{-1}, respectively, C-O-C epoxy at 1046.34 cm^{-1}, -CH_2 bending at 732.13 cm^{-1}, and C—C rocking vibration at 710.23 cm^{-1}. These shifts are attributed to the entry of RGO into the PCL matrix and matrix-filler interactions in the literature [9]. In addition, the C═O stretching vibration of the carbonyl group at 1720 cm^{-1} and the C—C rocking vibration bands at 710.23 $cm^{-1}$are attributed to the presence of PCL in RGO-containing nanofibers [9]. In the FTIR spectrum of PCL/RGO nanofibers shown in Fig. 2(a), bands belonging to -OH (hydroxyl) at the wavenumber of 3444.89 cm^{-1}, C—H bending at 1470.95 cm^{-1},

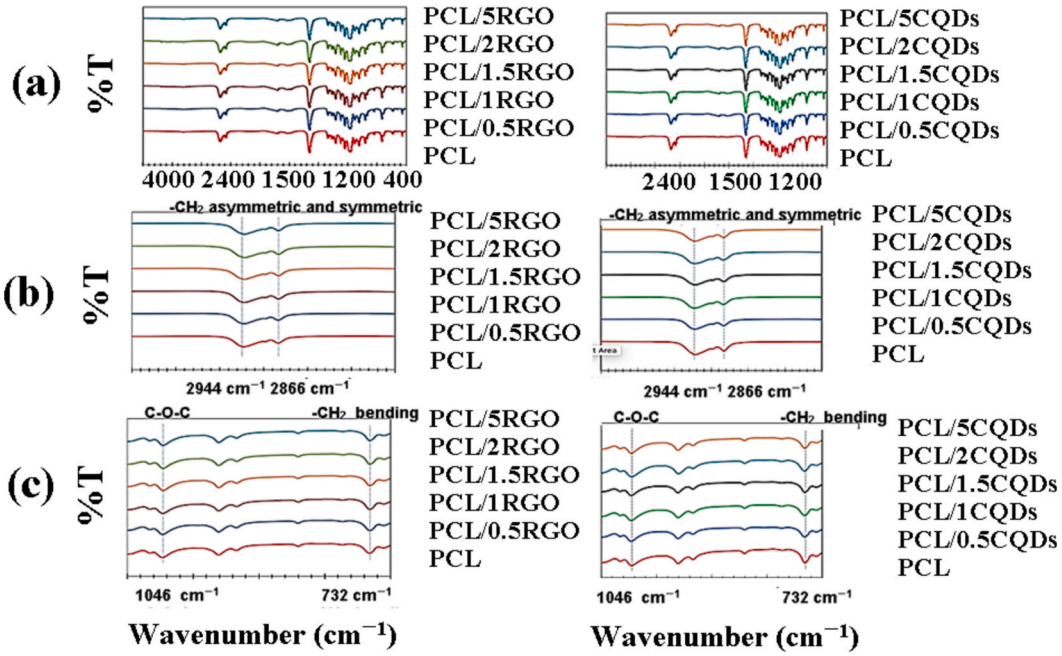

Fig. 2. (a) The FTIR spectra of PCL nanofibers correspond to all vibration peaks.
(b) FTIR spectra of PCL nanofibers corresponding to CH_2 asymmetric and symmetric vibration peaks, and (c) The FTIR spectra of PCL nanofibers correspond to the bending vibration peaks of C-O-C epoxy and CH_2.

C—H wagging at 1365.16 cm^{-1}, C—C stretching at 1293.64 cm^{-1}, C-O-C asymmetric stretching at 1238.80 cm^{-1}, and C-O-C symmetric stretching vibrations at the wavenumber of 1164.09 cm^{-1} were also detected. Researchers have seen the same functional group bands in the FTIR spectrum in other nanofiber studies. These studies added different types of graphene (graphene oxide (GO), RGO) to the PCL matrix [7,12,28–30]. The CH_2 bending vibration at 732.13 cm^{-1}, as shown in Fig. 2(c), exhibited a reduction in band intensity and a shift towards a lower wavenumber in all nanofibers. FTIR research of Pebdeni et al. [31] on CQDs-based PCL/CQDs nanofibers derived from *o*-phenylenediamine revealed that the interactions between PCL-CQDs may be responsible for the reduction in the intensity of the functional group bands. This study identified the interaction between PCL and CQDs through a decrease in intensity and a shift towards a lower wavenumber in the CH_2 bands across all nanofibers. Fig. 2(b) shows a shift in the bands belonging to the C-O-C epoxy group, observed at 1046.34 cm^{-1}, to lower wavenumbers in all nanofibers. It was also detected decreases in the wavenumber values of the bands associated with the C-O-C epoxy and CH_2 bending groups, located at 1046.34 cm^{-1} and 732.13 cm^{-1}, respectively, in the PCL/RGO nanofibers. This result shows that both the RGO filler and the CQD filler interact more with the CH_2 and C-O-C groups of PCL. It was determined that the bands of C-O-C symmetric stretching at 1160 cm^{-1}, C—C stretching at 1292.92 cm^{-1}, C—H shearing at 1363.81 cm^{-1}, and C—H stretching vibrations at 3443.21 cm^{-1} of PCL/2CQDs nanofiber shifted to lower wavenumbers compared to the FTIR spectra of the same functional groups of PCL and other nanofibers. This result shows that adding 2.0 wt% CQDs provides more interaction with PCL than other addition amounts. The overlapping of PCL, RGO, and CQDs bands within the nanofibers is responsible for the changes not clearly visible in the FTIR spectra of RGO and CQDs filled PCL nanofibers in Fig. 2(a) [5,15].

The results obtained from the XRD analysis of PCL nanofibers are given in Table 2 and the XRD diffractograms are provided in Fig. 3(a-b). Table 3 and Fig. 3(a) show that the (110) and (200) planes have peaks at $2\theta^\circ = 21.4^\circ$ and 23.8°. These peaks show that PCL has a semi-crystalline structure. Previous studies [32,33] have demonstrated that these two characteristic peaks are part of the orthorhombic structure of PCL. Fig. 3 (b) shows the increases and decreases in the intensities of the peaks belonging to the (110) and (200) planes reflecting the crystal structure of PCL, as well as the shifts in $2\theta^\circ$ values seen in the XRD diffractogram

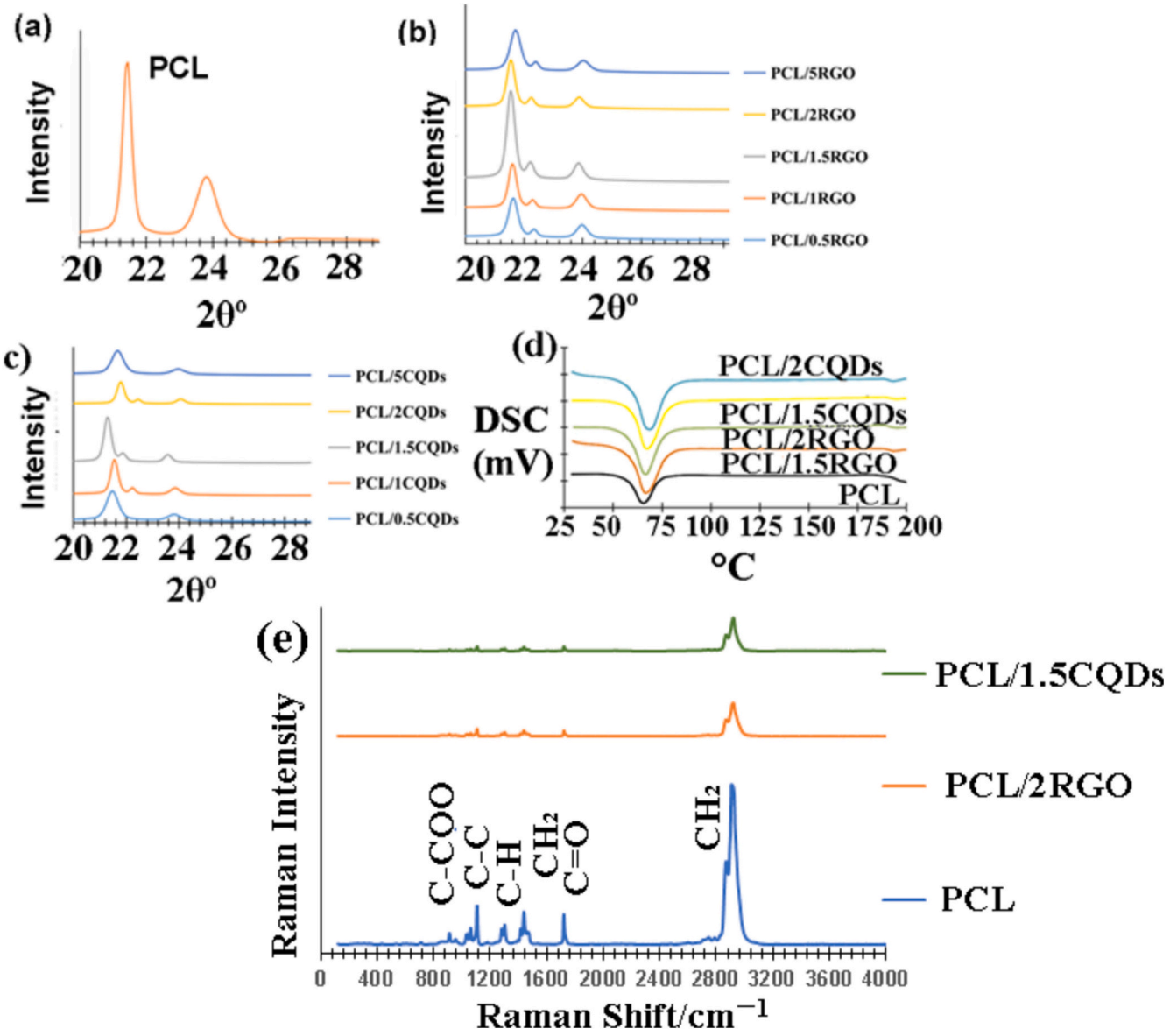

Fig. 3. XRD patterns of (a) PCL, (b) PCL/RGO nanofibers, (c) PCL/CQDs nanofibers, (d) DSC thermograms of PCL nanofibers and (e) Raman spectra of PCL nanofibers.

Table 3
D-spacing, crystallite size, and micro-strain of PCL nanofibers.

Nanofibers	2θ°	D-spacing (Å)	Crystallite size (Å)	Micro-strain (%)
PCL/0.5RGO	21.677	4.09983	253.7201	0.807943
	24.0168	3.70545	222.0705	0.834296
PCL/1RGO	21.6031	4.11369	297.7017	0.690908
	23.9447	3.71643	222.0414	0.836878
PCL/1.5RGO	21.5974	4.11476	297.699	0.691094
	23.9008	3.72316	254.6873	0.730928
PCL/2RGO	21.5455	4.12456	297.6744	0.692797
	23.8718	3.72762	254.674	0.731841
PCL/5RGO	21.7013	4.09529	221.1837	0.925766
	24.0131	3.70601	196.8951	0.941114
PCL	21.414	4.14958	297.6124	0.697145
	23.7906	3.74016	125.8231	1.486279
PCL/ 0.5CQDs	21.4651	4.13983	176.1072	1.175371
	23.8028	3.73828	160.5297	1.164356
PCL/1CQDs	21.5421	4.12519	297.6728	0.692906
	23.8399	3.73255	221.9992	0.840666
PCL/ 1.5CQDs	21.2849	4.17445	297.552	0.701466
	23.562	3.77593	298.6806	0.632102
PCL/2CQDs	21.7775	4.08114	297.7849	0.685249
	24.0469	3.70088	254.7546	0.726362
PCL/5CQDs	21.6629	4.10246	176.1643	1.164385
	23.9544	3.71496	160.5742	1.156774

of PCL nanofibers obtained with varying wt% RGO additions. Fig. 3(b) clearly shows the increase in the peak intensity of the (110) plane of the PCL/1.5RGO nanofiber compared to other graphene-containing nanofibers. In the literature, the increase in peak intensity in nanofiber studies obtained by adding graphene derivatives to the PCL matrix has been associated many times with the structure's crystallinity [34]. The decline in the peak intensity of the (110) plane detected in the XRD examination of the nanofibers generated by incorporating graphene into the PCL matrix was ascribed by Fakhrali et al. [35] to the reduction in the crystallinity of the structure. Table 3 compares the 2θ° values of the PCL nanofiber with all the nanofibers containing RGO. Significant shifts are observed. The changes seen in both the increase in intensity and the 2θ° values suggest that RGO has an effect on how crystallized PCL is. In their study, Güngördü Er et al. [36] found that the crystallinity levels of the nanofibers they synthesized were comparable. They did not detect any notable changes in the wavelengths that appeared in the XRD analysis of the PCL nanofibers with graphene derivatives. In this study, the crystallite size values for each degree in Table 3 are shown in dark color for the $2\theta^\circ = 21.4^\circ$ peak in 1.0 wt%; 1.5 and 2.0 wt% RGO doped nanofibers. For the $2\theta^\circ = 23.8^\circ$ peak in all wt% RGO doped nanofibers, a rise was seen compared to the pure PCL. It was achieved a 50.6 % increase in the crystallite size value, particularly at 1.5 and 2.0 wt% RGO contents, compared to the pure PCL. The XRD diffractogram of reduced graphene oxide (RGO) has a wide diffraction peak at $2\theta^\circ = 24^\circ$, which corresponds to the (002) plane. This peak indicates the amorphous structure of RGO [25]. Notably, the XRD diffractogram of all nanofibers in Fig. 5(b) did not exhibit a broad diffraction peak indicating the amorphous structure of RGO added to the PCL matrix. This result is attributed to the homogeneous distribution of graphene in the PCL matrix [35]. In the production and characterization studies of PCL/Gelatin/Graphene nanofibers reported by Heidari et al. [16], the characteristic peak of graphene was not observed in the XRD diffractograms of the nanofibers. They attributed this result to the interaction between graphene and the polymer matrix, as well as the homogeneous distribution of graphene in the polymer matrix. There was no significant change in the interlayer distance values; the microstrain values decreased as expected with the increase in crystallite size. The results obtained from the XRD analysis of PCL and PCL/CQDs nanofibers are given in Table 3, and the XRD diffractogram is given in Fig. 3(a-b). The XRD analysis section of PCL/RGO nanofibers elucidated the XRD diffractogram of the pure PCL in Fig. 6(a). Examining the XRD diffractogram of the CQDs filled nanofibers in Fig. 3(b) reveals changes in peak intensities and degrees, indicating changes in the crystallinity of the structure. Table 3 shows that the interlayer distance value of the crystal peak of the (110) plane of the pure PCL at $2\theta^\circ = 21.4^\circ$ increases at 1.5 wt% CQDs content. Table 3 revealed that the addition of RGO in micro size to the PCL matrix did not alter the interlayer distance in all instances, while the addition of 1.5 wt% CQDs in nano size to the PCL matrix enhanced the interlayer distance, indicating their inclusion in the PCL crystal structure. Rajaura et al. [37] reported that the increase in interlayer distance results in the incorporation of filler into the crystal structure of the polymer. As a result, 1.5 wt% CQDs content was the most effective additive amount on the crystal structure of PCL. As seen in Table 3, the crystallite size value of the peak belonging to the (110) plane started to increase with the addition of 1.0 wt% CQDs and reached its maximum value at 2.0 wt% CQDs content when compared to the pure PCL. It was reduced to 5.0 wt% CQDs content. The crystallite size value of the peak belonging to the (200) plane at $2\theta^\circ = 23.8^\circ$ started to increase with 0.5 wt% CQDs content and reached its maximum value at 1.5 wt% CQDs content with an increase of 57.9 %. As seen in Fig. 3(b), the PCL/1.5CQDs nanofiber has the highest peak intensity in both planes among all nanofibers, supporting the observed increase in crystallite size [38]. Microstrain values also decreased with the increase in crystallite size, as expected.

As a result of XRD and FTIR analysis of the produced PCL nanofibers, considering the crystal structure, crystallite size, and polymer-filler interactions within the nanofibers, nanofiber samples containing 1.5 and 2.0 wt% RGO and CQDs were selected, and other analyses were performed.

Fig. 3(d) shows the DSC analysis results of PCL nanofibers. As seen in Fig. 3, a sharp endothermic peak at 66.05 °C reflecting the crystal structure of PCL and the % crystallinity value of PCL in Table 4 are consistent with the DSC results of PCL nanofibers obtained by electrospinning method previously in the literature [39,40].

It is seen from Table 4 that the melting temperature and melting enthalpy values increased with the addition of RGO and CQDs, and the shifts in the melting peaks are seen from Fig. 3(d). It was also determined that the crystallinity degrees increased with the addition of RGO and CQDs. This result showed that both RGO and CQDs additives created a nucleation effect. In their study on PCL nanofibers produced with RGO additive at different voltage values, Correa et al. attributed the decrease in melting enthalpies and crystallinity degrees observed in DSC analyses of the nanofibers to the decrease in the mobility of the polymer chains of the RGO nanolayers and the formation of an amorphous structure [2]. The XRD analysis of the same nanofibers in this study revealed the crystal structure and increased the crystallite size values (Fig. 2(b); Table 3). Therefore, in this study, RGO and CQDs additives created an effect of increasing the crystallinity in the structure. The results of the XRD and DSC analysis supported this conclusion. The addition of RGO and CQDs to the PCL matrix increased thermal stability and provided polymer-filler interactions at all content amounts. The FTIR analysis results revealed that the PCL/2CQDs nanofiber, with an increase of 8.2 % compared to PCL, had the highest crystallinity degree and the highest polymer-filler interaction (Fig. 2(a-b-c). The DSC analysis attributed the increases in crystallinity degrees to their higher mechanical properties [41]. The mechanical properties section of this study reports the high

Table 4
DSC characteristics of PCL nanofibers.

Nanofibers	T_m (°C)	ΔH_m (J/g)	% Crystallinity
PCL	66.05	58.56	41.97
PCL/1.5RGO	68.92	60.12	43.75
PCL/2RGO	67.16	60.89	44.54
PCL/1.5CQDs	67.91	61.97	45.09
PCL/2CQDs	69.53	62.14	45.45

elastic modulus and nanohardness results of the produced nanofibers compared to the pure PCL. Fig. 3(e) shows the Raman spectra for pure PCL and PCL nanofibers. The C–COO group at 910 cm^{-1} and the ester C═O group at 1721 cm^{-1} are observed in the Raman spectra of pure PCL in Fig. 3(e). The weak absorption bands at 1060 cm^{-1}, 1110 cm^{-1}, 1299 cm^{-1}, and 1439 cm^{-1} are attributed to CH_2 vibrations, while the strong absorption band at 2915 cm^{-1} is attributed to CH_2 bending vibrations. These vibration bands are consistent with those reported in previous studies of PCL in the literature [9,16], as well as with the functional groups identified from the FTIR results of this study [Fig. 2]. In this study, as clearly seen in Fig. 3(e), the Raman spectra of the nanofibers obtained by adding RGO and CQDs to the PCL matrix exhibit the same bands as those of pure PCL, with only a decrease in their intensity. In the study by Iswarch et al., they added different amounts of RGO to the PCL matrix and attributed the appearance of PCL bands in the fiber samples to the successful formation of the composite. They also observed the disappearance of the D and G bands of RGO in the composite nanofibers, which they attributed to interactions between RGO and PCL. In the literature, the D and G bands of graphene at 1305 cm^{-1} and 1577 cm^{-1}, respectively [16], were not observed in the Raman spectrum of the PCL/

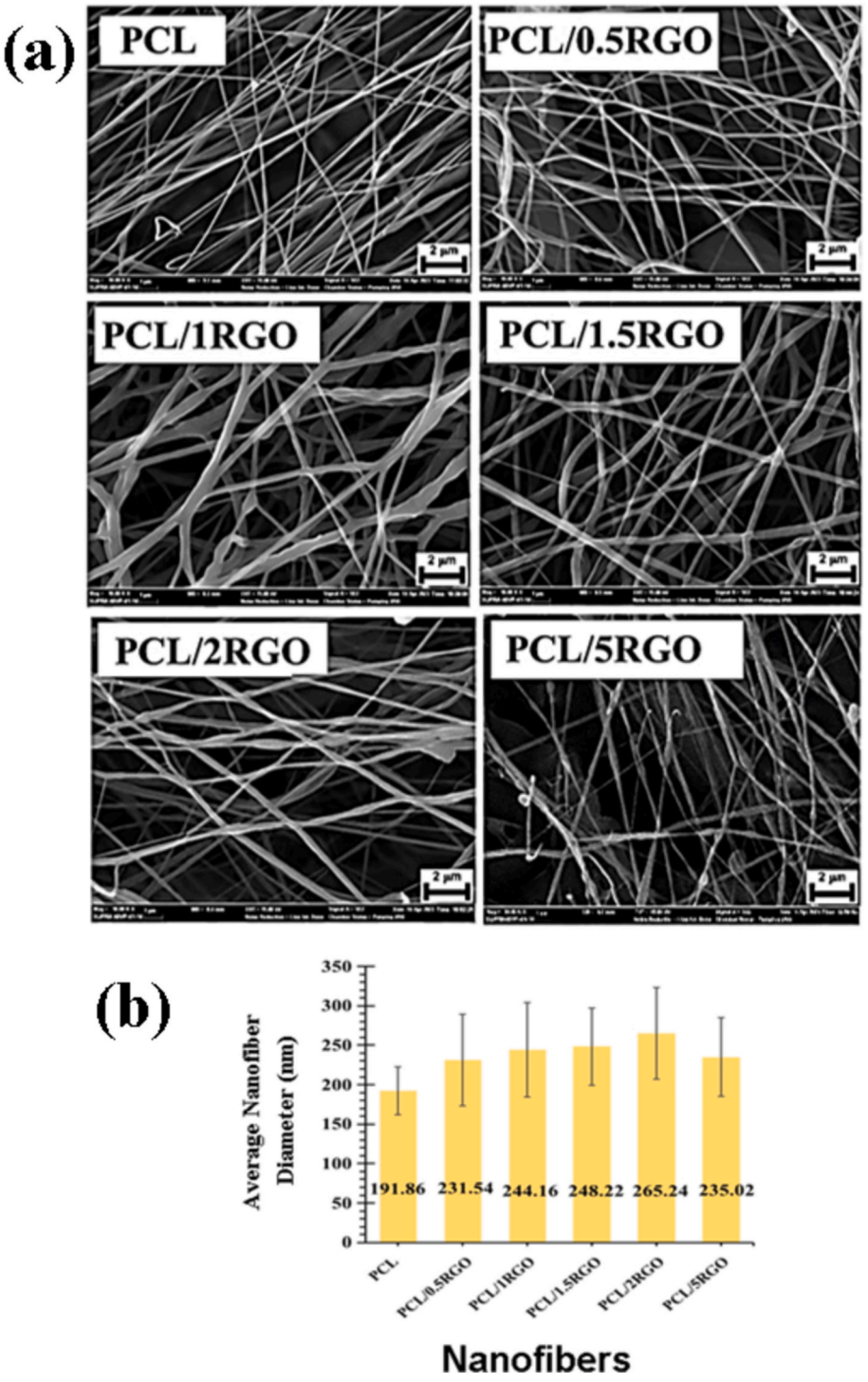

Fig. 4. (a) FE-SEM images and (b) Average nanofiber diameter of PCL and PCL/RGO nanofibers.

RGO nanofiber sample in this study. These results are consistent with the FTIR findings, which further support the existence of interactions between PCL and the RGO and CQDs fillers.

The electrospinning method successfully produced homogeneous-sized and bead-free structures for each nanofiber, as shown in Fig. 4 (a). The presence of beads on the scaffolds produced by electrospinning is undesirable because it greatly reduces the scaffold surface/volume ratio [42]. Fig. 4(b) presents the average nanofiber diameter values derived from FE-SEM images of PCL and PCL/RGO nanofibers. Fig. 4(b) shows that the addition of RGO increased the nanofiber diameters up to 5.0 wt%. The average nanofiber diameter of the pure PCL nanofibers increased from 191.86 nm to 265.24 nm for the nanofiber containing 2.0 wt% RGO. Gohari et al. [12] also reported an increase in nanofiber diameter with an increase in RGO addition in the PCL matrix. They explained this increase by strengthening π-π interactions as the distance between the RGO layers decreases. Fig. 4(b) shows a decrease in the nanofiber diameter at 5.0 wt% RGO content. The study by Faraji et al. [7] reported a decrease in the nanofiber diameter with an increase in the GO concentration in the PCL matrix. They explained the decrease in nanofiber diameter with the increase in electrical conductivity. In addition, Correa et al. [2] evaluated the decrease in nanofiber diameter and the increase in electrical conductivity in their tissue scaffold studies with RGO and PCL. Researchers reported that the RGO layers were responsible for the increase in conductivity, and at higher RGO contents, they would obtain a greater number of contacts between the layers, thereby enabling electron and ion mobility with a better internal network. Additionally, the same study determined a decrease in the electrical conductivity of the composites containing the highest RGO, and associated this decrease with the deterioration of the internal network due to agglomeration. This study also attempted to explain the observed increases and decreases in the nanofiber diameters through the use of electrical conductivity tests. Table 5 shows the electrical conductivity measurement results of PCL nanofibers. Table 5 reveals that the pure PCL nanofiber demonstrated a low conductivity value of $1.20318.10^{-9}$ S/cm. This result is consistent with the conductivity results of PCL nanofiber in the literature [43]. The conductivity value of $9.49045.10^{-10}$ S/cm of the nanofiber containing 1.5 wt% RGO was found to be lower than that of the pure PCL nanofiber. This result is consistent with the results of decreasing conductivity with increasing nanofiber diameter in the literature [44]. The nanofiber with 2.0 wt% RGO, on the other hand, was more conductive than the PCL and PCL/1.5RGO nanofibers, even though it had a bigger diameter. Its conductivity value was $1.43312.10^{-8}$ S/cm. The nanofiber containing 5.0 wt% RGO was found to have the highest conductivity among the RGO-containing nanofibers, with a conductivity value of $1.75159.10^{-8}$ S/cm. Despite the PCL/5RGO nanofiber's decreasing diameter, the observed increase in conductivity showed a good internal network with no agglomeration, even at the highest RGO content. All doped nanofibers demonstrated insulating properties. Shabankhah et al. [45] found that the conductivity values of PCL/GO tissue scaffolds with a 3D printer increased from $1.07 \pm 0.09.10^{-8}$ S/m to $2.75 \pm 0.094.10^{-4}$ S/m with the addition of GO. And they found that this measured change was further increased by the addition of gelatin ($1.49 \pm 0.2.\ 10^{-2}$ S/m). However, the reported values were still low. Jaymand et al. [46] reported that due to the insulating properties of PCL, it would be difficult to reach even 10^{-5} S/cm in materials with high PCL content.

Table 5
Electrical conductivity of PCL and PCL nanofibers.

Nanofibers	Electrical conductivity sigma (S/cm)
PCL	$1.20318.10^{-9}$
PCL/1.5RGO	$9.49045.10^{-10}$
PCL/2RGO	$1.43312.10^{-8}$
PCL/5RGO	$1.75159.10^{-8}$
PCL/1.5CQDs	$4.80255.10^{-9}$
PCL/2CQDs	$1.77707.10^{-8}$
PCL/5CQDs	$1.85987.10^{-8}$

Fig. 5(a) demonstrates the formation of homogeneous-sized and relatively bead-free nanofibers. Ghosal et al. [47] investigated the antibacterial properties of nanocomposites containing hydrophobic CQDs and saw small amounts of beads forming in images of nanofibers. In Fig. 5(b), it was determined that nanofiber diameters tended to decrease with the increase in wt% CODs content in the PCL matrix. Ghorghi et al. [5] also reported decreases in nanofiber diameters with an increase in CQDs content in their nanocomposite tissue scaffold studies. Furthermore, the same study reported that a decrease in nanofiber diameter influences cell behavior, leading to an increase in cell growth and adhesion. Increasing the electrical communication between cells can improve the performance of the tissue engineering scaffold, as the electrical conductivity of the scaffold plays an important role in controlling cell behavior. Jaymand et al. [46] conducted electrical conductivity measurements on nanofiber samples containing CQDs, similar to RGO-doped nanofibers, and Table 5 presents the conductivity measurement results. Table 4 reveals that the PCL/1.5CQDs nanofiber exhibits higher conductivity than the pure PCL nanofiber, with a conductivity value of $4.80255.10^{-8}$ S/cm. This result also explains the decrease in the fiber diameter of the same nanofiber. The conductivity ($1.77707.10^{-8}$ S/cm) of PCL/2CQDs nanofiber kept going up, while the diameter of the nanofiber got smaller at the same time. Although the conductivity value of the PCL/5CQDs nanofiber containing the highest CQDs continued to increase, the nanofiber diameter decreased slightly. The addition of CQDs to the PCL matrix increased the electrical conductivity, resulting in a decrease in the nanofiber diameter. In the literature, nanofiber samples containing CQDs also exhibited same results [15].

3.2. Mechanical analysis results

In Fig. 6(a), it is seen that the elastic modulus values are higher in the nanofibers containing CQDs compared to the pure PCL nanofiber from the beginning of the nanohardness measurement. It is seen from Fig. 6(a) that, except for the oscillation seen in the elastic modulus values of the PCL/1.5RGO nanofiber sample as the depth increases, the other nanofibers exhibit different elastic modulus values without oscillation with the increase in depth. The changes observed in the nanohardness values of PCL and PCL nanofibers as the depth increases are examined in Fig. 6 (b); it is seen that the nanofibers containing CQDs exhibit high nanohardness values as in the elastic modulus change from the beginning. Especially in the first 110 nm section in the nanofibers containing RGO, fluctuations in the nanohardness values were observed with the increase in depth compared to the nanofibers containing CQDs. It is thought that there are two different reasons for this result. The first is that the RGO distribution in the nanofibers exhibits a less homogeneous distribution compared to the CQDs distribution, and the second is that the RGO added to the PCL matrix is not nanosized. Tyagi et al. [48] studied the nanomechanical properties of PCL/hydroxyapatite (HA) nanofibers made by electrospinning. They found that the sudden rise in the elastic modulus of a certain amount of HA addition was due to the particles becoming less evenly distributed and the indenter tip hitting areas that were rich in HA particles or poor in HA particles. In this study, the analysis (XRD, FTIR, SEM, electrical conductivity, DSC) revealed that RGO is distributed homogeneously in the polymer matrix. Therefore, the changes seen in the RGO-containing nanofibers during this test are not due to the fact that the RGO is not evenly distributed in the PCL matrix. It is known that nanohardness data are normally collected from very small areas on the nanofiber surface, and these examined areas are likely to be heterogeneous in terms of amorphous and crystalline regions, therefore, it is thought that the results obtained from nanofibers containing RGO may not be representative of their macro-mechanical properties. A similar result was reported in the study of Gloria et al. [49] on tissue scaffold samples produced with PCL. Fig. 6(c) shows a 73 % increase in PCL/1.5CQDs nanofiber and a 36 % increase in PCL/

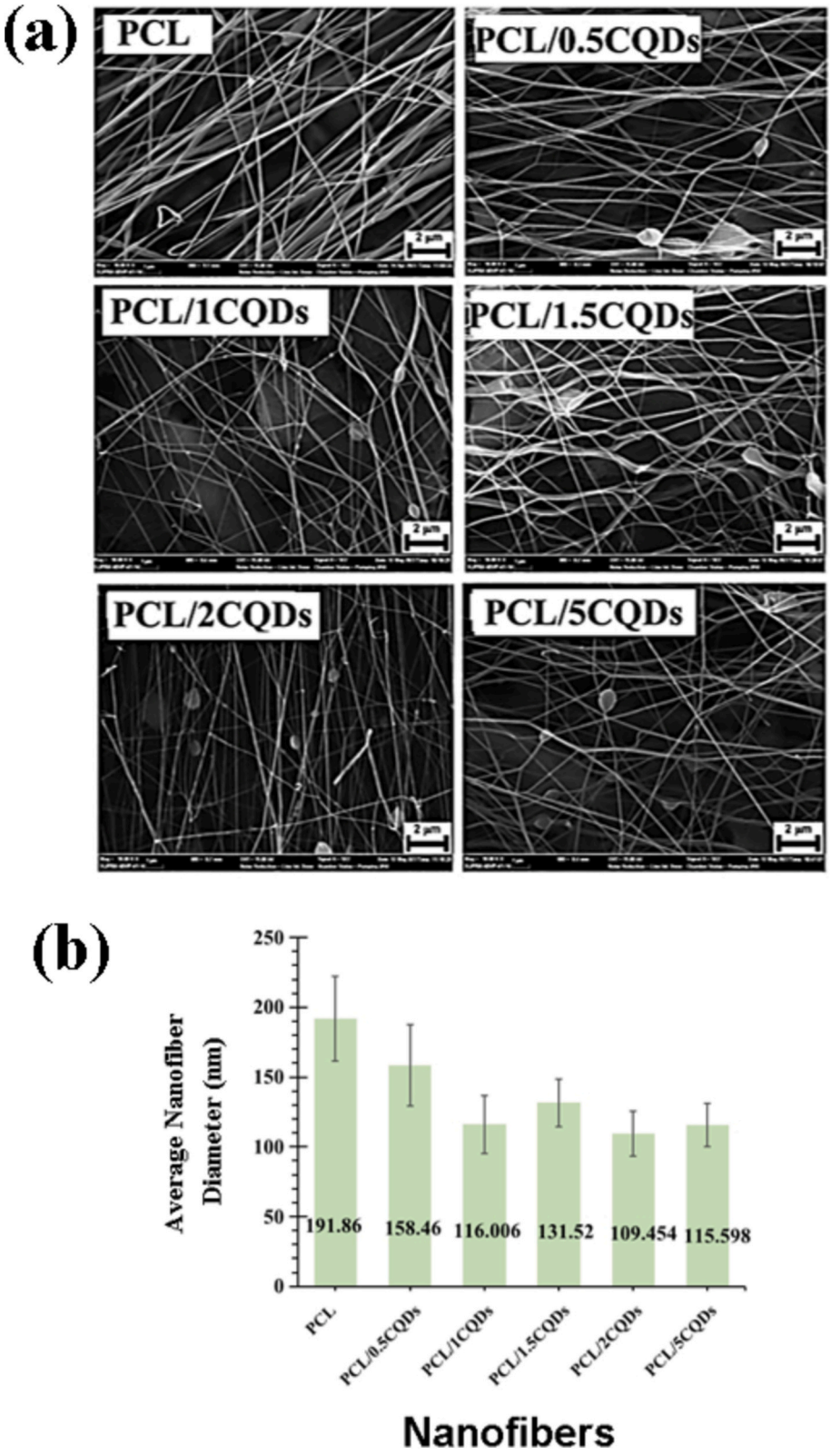

Fig. 5. (a) FE-SEM images and (b) Average nanofiber diameter of PCL and PCL/CQDs nanofibers.

2CQDs nanofiber when compared to the elastic modulus value of pure PCL nanofiber. In the nanofiber samples containing RGO, a 16 % decrease was detected in PCL/1.5RGO nanofiber and a 1.9 % increase in PCL/2RGO nanofiber. It was determined that all nanofibers had higher nanohardness values compared to the pure PCL nanofiber. The PCL/1.5CQDs nanofiber sample showed the highest increase at 160 %, followed by the PCL/2CQDs nanofiber sample at 140 %, and the PCL/1.5RGO and PCL/2RGO nanofibers at 40 %. The results of PCL nanofiber studies conducted in the literature were consistent with the values found in this study for the pure PCL nanofiber [50,51]. The improvements

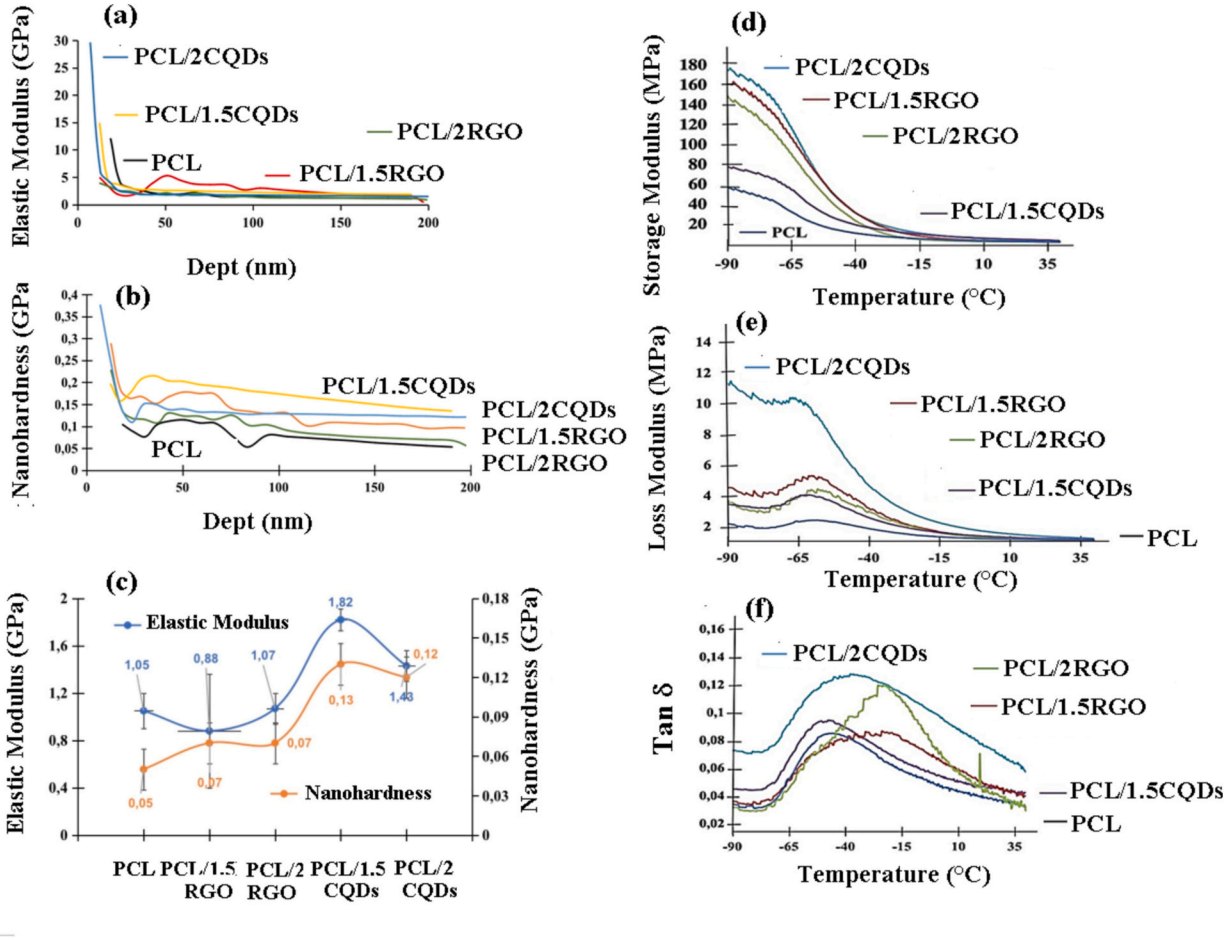

Fig. 6. (a) Effect of depth on elastic modulus, (b) Effect of depth on nanohardness, (c) Elastic modulus and nanohardness values (d) Storage modulus, (e) Loss modulus and (c) Tan δ curves of PCL nanofibers.

observed in nanomechanical properties in the literature have been attributed to the fact that fillers homogeneously distributed in the PCL matrix can provide load transfer and that additives act as nucleation centers with increasing crystallinity [52]. The higher crystallinity levels found in DSC and XRD analyses of CQDs filled PCL nanofibers compared to RGO filled nanofibers (Tables 2 and 3) support the high improvement in mechanical properties compared to RGO filled nanofibers. In particular, PCL/1.5CQDs nanofiber has the highest nanohardness and elastic modulus values, is the only nanofiber sample included in the crystal structure of PCL in XRD analysis, which is also explained by the increase in the interlayer distance value (Table 2). The change in the storage modulus of pure PCL and PCL nanofibers with temperature is seen in Fig. 6(d). The storage modulus curve of PCL nanofiber showed a sharp decreasing trend between −90 °C and − 30 °C. This temperature range represents the main relaxation process and corresponds to the amorphous PCL regions associated with the PCL glass transition. Between −30 °C and 40 °C, the storage modulus decreased further due to the progressive softening of the PCL matrix. Here, amorphous and crystalline regions coexist. At higher temperatures between 45 °C and 70 °C, the storage modulus is expected to decrease sharply due to complete melting of PCL crystal domains, as observed from the DSC thermogram of PCL (Fig. 3(d)). In the storage modulus curve in Fig. 6(d), it is seen that the storage modulus values of RGO and CQDs filled nanofibers are higher than the pure PCL in both the glassy region and the rubber region. This result is attributed to the fact that in all nanofibers, the RGO and CQDs filled nanofibers are distributed in the matrix without agglomeration and that voids are not formed even as the temperature increases within the structure by providing polymer-filler interaction and causing an increase in hardness in the matrix [53,54]. Frone et al. [55] attributed the increased storage modulus value as a result of the DMA analysis in their study to better stress transfer and better interaction with the polymer matrix by the cellulose nanocrystal-added nanofibers. They also reported that the increase in the hardness of the polymer matrix caused by the same nanofibers was consistent with the tensile test results. The nanoindentation test results of this study also showed results compatible with DMA analysis. The elasticity of the material influences the storage modulus, whereas the viscosity of the material influences the loss modulus. According to Fig. 6(d) and 6(e), both storage modulus and loss modulus of PCL increased with RGO and CQDs contents. Mi et al. [53] reported that adding cellulose nanocrystals (CNC) to PCL matrix improved the storage modulus of nanofibers more than the loss modulus, and that CNC additives affected the elastic part of PCL more. In this study, it was determined that the increase values in the storage modulus of all nanofibers were less than the increase values in the loss modulus; for example, PCL/2CQDs nanofiber, which has the highest storage and loss modulus values, provided a 210.79 % increase in storage modulus and a 595.27 % increase in loss modulus compared to pure PCL. Therefore, it is thought that the RGO and CQDs additives used in this study are more effective on the crystalline region than the elastic part of PCL. The XRD (Tables 2) and DSC analysis results of the nanofibers (Table 3) also support this result. The XRD and DSC analysis results revealed an increase in crystallinity, and the addition of RGO and CQDs led to a nucleation effect. The literature reports that nanofillers distributed in the amorphous regions of the polymer cause low crystallinity [56,57]. Salgado et al. [58] associated the decrease in storage modulus in the DMA analysis of PCL/sebacic acid gels with the decrease

in the crystalline phase of the gels and the fact that this polymer has more elastomeric properties compared to pure PCL. In this study, the increase in crystallinity (Tables 3 and 4) supported the increases in storage modulus (Fig. 6(d)). In addition, they reported that the sample that had more degradation also presented higher storage modulus values. The biodegradability test results section of this study will explain that the nanofiber sample with the highest storage modulus value (PCL/2CQDs) exhibited the highest biodegradability (Fig. 7(a)). The PCL nanofiber loss modulus as a function of temperature showed a maximum peak at −61.05 °C, and this maximum temperature was defined as the glass transition temperature of PCL (Fig. 6(e)). Srinivasa et al. [59] reported in their PCL nanofiber study that they determined the glass transition point as the maximum point of the loss moduli curve. The glass transition temperatures of RGO and CQDs filled PCL nanofibers determined from the loss moduli curve as a function of temperature are given in Table 6. Table 6 indicates that the glass transition temperature of nanofibers including RGO increased by 2–4 °C relative to pure PCL, while the glass transition temperature of nanofibers containing CQDs remained equivalent to that of PCL. The elevation of the glass transition temperature was ascribed to the superior interfacial adhesion produced by the RGO filler in comparison to the CQDs filler within the polymer matrix [55]. In Fig. 6(f), the damping modulus (Tan δ) curve presents a single well-defined relaxation peak around −50 °C, corresponding to the relaxation of the amorphous component of PCL, which is the main component in the matrix. The higher damping modulus values of the nanofibers than the neat PCL nanofibers are attributed to the presence of polymer-filler interfacial interactions [55]. All nanofibers, except for PCL nanofibers, exhibit broadened Tan δ peak shapes. The literature reports the broadening of the Tan δ peak as a strong indicator of the interaction between the polymer-filler components [60]. Fig. 6(f) illustrates that all nanofibers have both soft and elastic characteristics at ambient temperature (25 °C). It was established that all nanofibers exhibit exceedingly low Tan δ values at ambient temperature. The Tan δ values, ranked from lowest to highest, are as follows: PCL (0.029), PCL/2RGO (0.035), PCL/1.5CQDs (0.040), PCL/1.5RGO (0.042), and PCL/2CQDs (0.076). Luo and Mater [61] found that the Tan δ value of the PCL composite they developed was as low as 0.067, indicating that the material exhibited both softness and elasticity at room temperature.

Table 6
The glass transition temperature of PCL nanofibers.

Nanofibers	Glass transition temperatures (°C)
PCL	−61,05
PCL/1.5RGO	−60,02
PCL/2RGO	−60,55
PCL/1.5CQDs	−61,87
PCL/2CQDs	−62,15

3.3. Biological analysis results

The degradation characteristics of PCL, PCL/RGO, and PCL/CQD nanofibers were examined at 37 °C in phosphate buffered solution (PBS) for a period of 56 days. Fig. 7(a) illustrates the variations in weight loss percentages according to the measurement days. The hydrophobic composition of pure PCL results in a degradation period of up to two years in body fluids [12]. The biodegradation of PCL occurs through hydrolysis. In comparison to other biocompatible and biodegradable polymers, it exhibits a reduced degradation rate attributable to the lack of hydrophilic groups and its semi-crystalline structure. Therefore, it is known as a polymer with high potential in preserving the integrity of the tissue scaffold [16]. As shown in Fig. 7(a), PCL achieved a very low weight loss of 0.93 % at the end of 56 days. In the literature, the biodegradation rate of PCL composites produced by adding different fillers to PCL increases depending on the hydrophilicity of the added filler [12]. Compared to the pure PCL, it is observed that the hydrophilic RGO and CQDs fillers added to PCL at 1.5 and 2.0 wt% increase biodegradability. Fig. 7(a) reveals that the nanofibers containing 2.0 wt

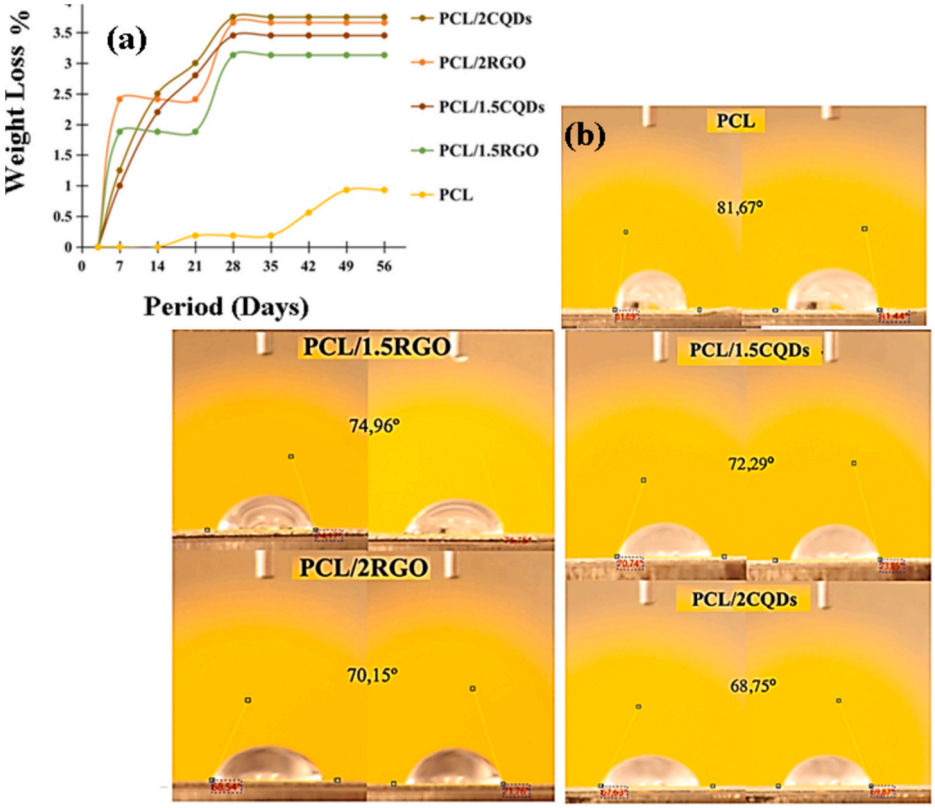

Fig. 7. (a) 56-day weight loss of PCL and PCL nanofibers in PBS solution (b) Contact angles.

% RGO and 2.0 wt% CQDs experienced the highest weight loss values at the end of 56 days, with degradation values of 3.66 % and 3.75 %, respectively. It was determined that nanofibers containing CQDs and RGO significantly increased the degradation of PCL. Fig. 7(a) specifically shows that nanofibers containing CQDs exhibited faster degradation on the 14th and 21st days compared to those containing RGO. Previous studies have reported the functional groups contained in RGO and CQDs used in this study [18,19]. This result is consistent with the findings of Aidun et al. [8] in their GO/chitosan/collagen/PCL nanofiber study, which reported that the GO-containing scaffold did not biodegrade much until the second week due to its chemical and mechanical properties, but that biodegradation accelerated with the penetration of liquid after the third week. Ghorghi et al. [5] reported that the hydrophobic structure of pure PCL led to the slowest degradation rate in the biodegradation test results, whereas the wettability of the surface of CQD-doped nanofibers resulted in higher weight losses. This study also conducted contact angle measurements on the nanofibers to better understand the biodegradation behavior of the produced nanofibers. Fig. 7 (b) compares the contact angle measurement images of PCL/RGO nanofibers with those of pure PCL nanofiber. PCL nanofiber had the highest contact angle value of 81.67°, reflecting its hydrophobic nature compared to other nanofibers. The literature reported that the electrospinning method produced PCL nanofiber with a contact angle of 85.00 [3]. It has also been reported in the literature that PCL has hydrophobic properties, and its contact angle is determined to be between 74 and 78° [62]. Fig. 7(b) shows that the PCL/2RGO nanofiber had the lowest contact angle value of all the nanofibers that contained RGO. It was found to be 70.15°. RGO's oxygen-containing functional groups transform PCL's hydrophobic structure into a hydrophilic state, leading to this result. In their contact angle measurement results, Rostami et al. reported that PCL/GO nanofibers have fewer contact angle degrees than pure PCL. The same study also stated that reducing the hydrophobicity of PCL with GO content enhances its bioactivity in tissue engineering applications by enhancing the nanofiber's various binding abilities [28]. Heidari et al. [16] attributed the increase in the hydrophilic character of the PCL/GO nanofibers to the oxygen-containing functional groups of GO, improving the surface polarity, and the possibility of forming hydrogen bonds. Fig. 7(b) shows the contact angle measurement images of PCL and PCL/CQDs nanofibers. As the CQDs content increased, the contact angle value decreased. At 2.0 wt% CQDs content, the lowest contact angle value was determined to be 68.75°. It was understood that the structure with a decreased contact angle compared to the contact angle of PCL is hydrophilic, as the CQDs filler, like RGO, possesses oxygen-containing functional groups. The study by Ghorghi et al. [5] found that the contact angle measurements of the PCL/CQDs nanofibers made from a mixture of citric acid and ethylenediamine in the PCL matrix greatly improved the tissue scaffolds' ability to attract water because CQDs are water-loving. The hydrophilic surface of the scaffolds facilitated bone cell adhesion, proliferation, and migration. Comparison of the contact angle data indicated that nanofibers including CQDs exhibited a more hydrophilic structure than those containing RGO, as illustrated in Fig. 7(b). The nanofibers' biodegradability test results, shown in Fig. 7(a), also reflect this result. The nanofibers containing CQDs degraded faster than those containing RGO. According to the biodegradability and contact angle results, the addition of RGO and CQDs disrupted PCL's hydrophobic nature, made the nanofiber structure hydrophilic, and increased PCL's degradation rate.

A 7-day examination was conducted in simulated bodily fluid (SBF) to assess the capacity of nanofibers to generate hydroxyapatite. Table 7 presents the EDS analysis results of nanofibers removed from the solution at the conclusion of day 1. Table 7 shows that by the end of the first day, the Ca and P percentages in the EDS analysis showed any hydroxyapatite formation. The Ca/P ratios at the end of the first day were PCL 0.057 %, PCL/1.5RGO 0.090 %, PCL/2RGO 0.038 %, PCL/1.5CQDs 0.267 %, and PCL/2CQDs 0.109 %. These results showed that 1 day was not sufficient for hydroxyapatite formation. Table 6 provides the FE-

Table 7
EDS analysis results of nanofibers removed from the SBF solution at the end of the first day.

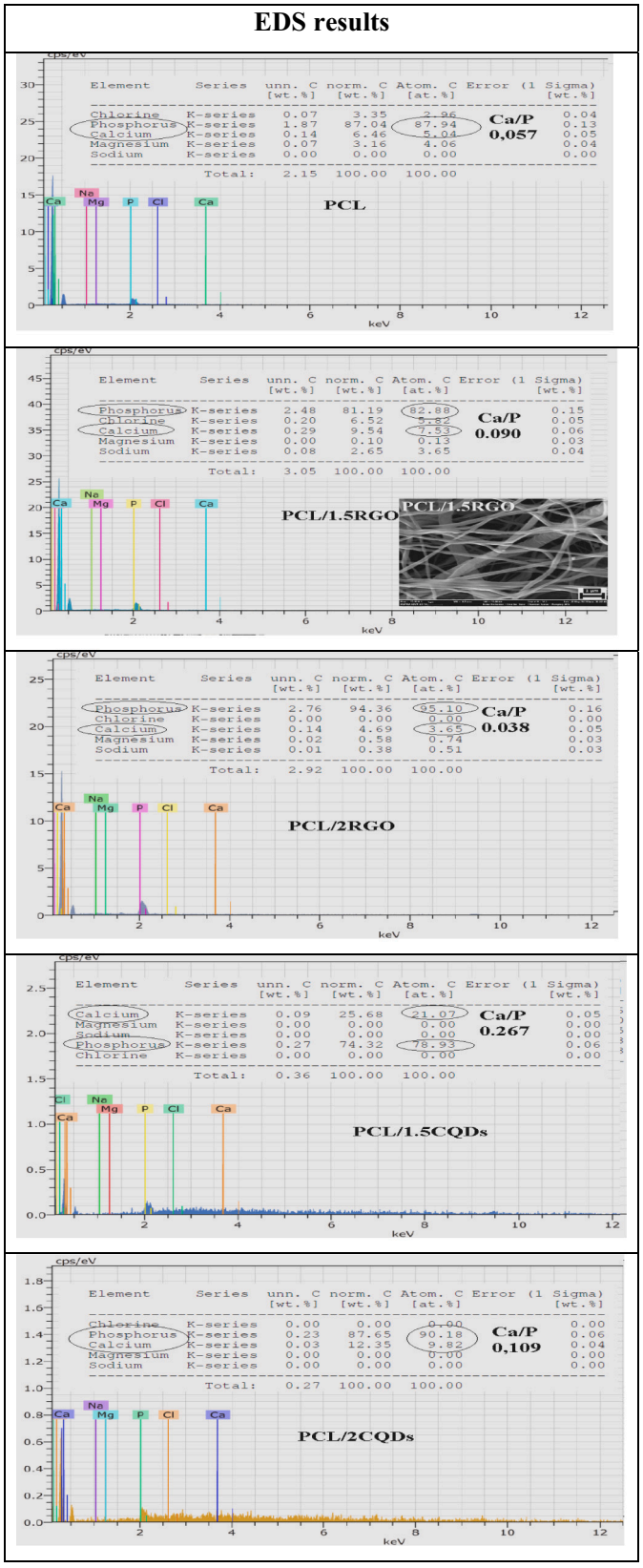

SEM image of one of the nanofiber samples. There is no trace of hydroxyapatite formation on the PCL/1.5RGO nanofiber surface. Gohari et al. [12] found in the bioactivity test results of PCL nanofibers they produced using RGO that the Ca/P ratio decreased as the RGO amount increased at the end of the first day, indicating a need for more time for hydroxyapatite formation. Yu et al. [24] reported that 7 days were sufficient for the formation of hydroxyapatite on nanofibers; they formed an amorphous structure in a short immersion time (1–2 days), which then transformed into crystalline hydroxyapatite. Examining the values from the EDS analysis result in this study revealed that the PCL/1.5CQDs nanofiber had the highest Ca/P deposition rate. This result showed that at the end of the first day, hydrophilic CQDs increased the hydroxyapatite formation more than RGO.

Fig. 8 shows FE-SEM images and EDS analysis results of the nanofibers at the end of the 7th day. It was determined that at the end of the 7th day, all nanofibers, including PCL, provided hydroxyapatite

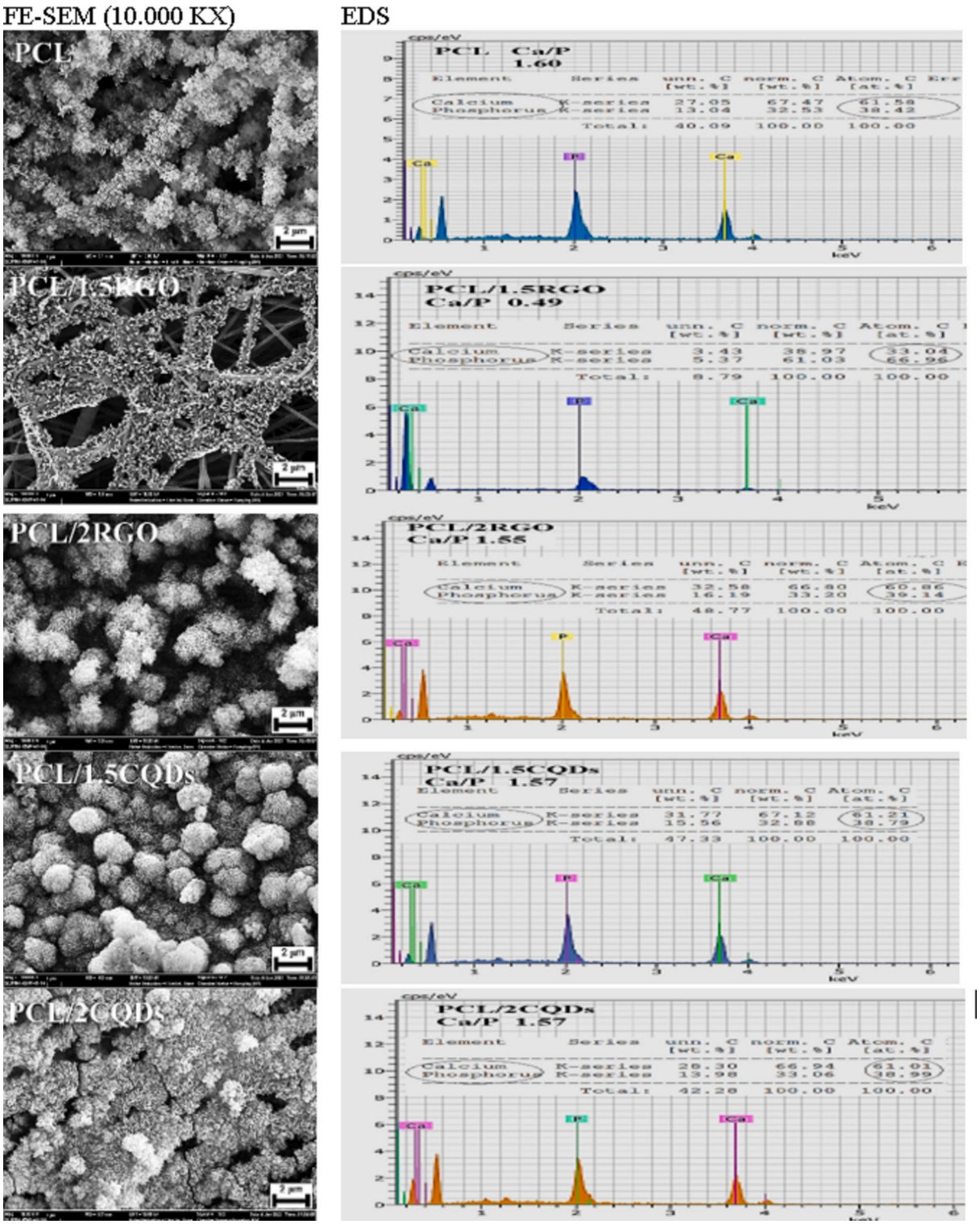

Fig. 8. FE-SEM images and EDS analysis of PCL nanofibers at the end of day 7.

formation. The surface images of the nanofibers in Fig. 8 closely resembled the apatite crystals depicting hydroxyapatite formation in the literature [12]. Gohari et al. [12] reported that the bioactivity test created negatively charged carboxylic acid groups (-COOH) that interacted with calcium and phosphate salts in SBF. This caused apatite crystals to form on PCL nanofibers. Furthermore, Fig. 8 presents the Ca/P ratios from the single point of the EDS analysis results, demonstrating the formation of hydroxyapatite. The calculated average values for multiple points were 1.60 % for PCL, 0.49 % for PCL/1.5RGO, 1.49 % for PCL/2RGO, 1.48 % for PCL/1.5CQDs, and 1.48 % for PCL/2CQDs. These results determined that the nanofiber containing 1.5 wt% RGO provided the lowest hydroxyapatite formation, while other nanofibers gave similar values, with PCL exhibiting the highest hydroxyapatite formation. These values are close to the Ca/P ratio in human bone, that is, the value of 1.68 given in the literature [8]. The literature attributes the anionic functional groups in the structure of GO, which enable the nucleation of calcium phosphates in PCL nanofibers produced using GO [30]. This study showed that the oxygen-containing functional groups of CQDs and RGO support the formation of hydroxyapatite at a value close to the calcium-phosphorus ratio of the bone. Afza et al. [63] reported the bioactivity test results of PCL nanofibers, indicating that the amount of both Ca and P elements increased as the immersion time increased, and lower Ca^{2+} nucleation and higher PO_3^{4-}adsorption occurred for 7 days, thus decreasing the Ca/P atomic ratio. This study determined that a similar situation occurred at 1.5 wt% RGO content, resulting in a very low Ca/P ratio compared to other nanofibers. The FE-SEM image of the same nanofiber clearly shows the differences that explain this result. This difference is reflected in the highly porous image of the nanofiber containing 1.5 wt% RGO.

At the end of the 1st day of the bioactivity test, XRD analysis was not performed because sufficient hydroxyapatite formation could not be observed in the FE-SEM/EDS analysis of the nanofibers. The XRD analysis results performed to prove the hydroxyapatite formation on the nanofibers at the end of the 7th day are given in Fig. 9. As seen in Fig. 9, sharp peaks belonging to the (211) and (222) planes seen at $2\theta^\circ = 32.8^\circ$ and 44.7° belonging to hydroxyapatite were observed in all other nanofibers except the nanofiber containing 1.5 wt% RGO. In particular, PCL nanofibers clearly displayed hydroxyapatite peaks belonging to both planes, but only the 222 plane's hydroxyapatite peak sharply emerged in nanofibers containing 2.0 wt% RGO and 1.5 and 2.0 wt% CQDs. This study is consistent with the XRD peaks proving the formation of hydroxyapatite in the bioactivity test results conducted on PCL nanofibers in the literature [8]. The FE-SEM images of the hydroxyapatite formed on the nanofiber surfaces in Fig. 8, along with the Ca/P ratios obtained from the EDS analysis, align with the XRD analysis

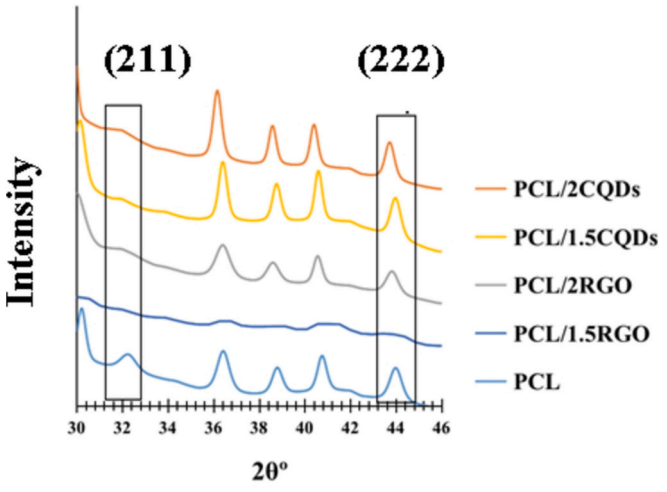

Fig. 9. XRD Diffractograms of PCL nanofibers at the end of day 7.

results of the same nanofibers. The nanofiber containing 1.5 wt% RGO exhibits a very low Ca/P ratio in the EDS analysis, and the XRD analysis reveals very low hydroxyapatite peaks. Aidun et al. [8] reported that the formation of hydroxyapatite in their PCL nanofiber study with GO is provided by the orientation of Ca^{+2} ions to the hydroxyl groups in the structure of GO. Previous studies have shown in the FTIR analysis results of the RGO and CQDs fillers used in this study that CQDs have more hydroxyl ion groups than RGO [18,19]. Therefore, the XRD diffractogram of both CQDs-containing nanofibers showed hydroxyapatite peaks, while the nanofiber containing 2 wt% RGO in the RGO-containing nanofibers showed the presence of clear peaks. Gohari et al. reported that apatite accumulation also depends on surface roughness [12]. This study found that the hollow structure in the FE-SEM image of the nanofiber containing 1.5 wt% RGO led to a decrease in apatite formation in this nanofiber. The conversion of the carboxyl group of PCL into the (COO^-) anion in the first hours of immersion in the SBF solution initiates the main mechanism for the crystallization of bone-like apatite on the surface of the PCL scaffold. This anion then supports the binding of calcium and phosphate ions, leading to the formation of bone-like hydroxyapatite [24,63].

According to the mechanical and thermal analysis results of PCL nanofibers, the antibacterial activity of PCL/2RGO and PCL/1.5CQDs nanofibers selected along with PCL nanofibers was tested by disk diffusion antibacterial analysis method. Fig. 10 presents the results of the antibacterial test. Fig. 10 reveals that neither PCL nor nanofiber samples exhibited antibacterial properties. Gram-negative bacteria (*Escherichia coli* Code: ATCC 25922) and gram-positive bacteria (*Staphylococcus aureus* Code: ATCC 25923) used for the antibacterial test were frequently used in previous PCL tissue scaffold studies [64]. It is known that PCL does not have antibacterial properties [65]. Therefore, it is tried to gain antibacterial properties by adding different antibacterial additives to PCL. For example, Aidun et al. [8] reported in their study that GO did not show antibacterial properties, while chitosan provided antibacterial properties in the study in which they examined the antibacterial activity of the nanofibers they obtained by adding GO and chitosan to the PCL matrix. The chemical structure is of significant importance for the way bacteria interact with surfaces. Previous and recent studies on the antibacterial and bacteriostatic properties of graphene, GO, RGO, and their composites reported advantages such as tuning the interaction with bacteria through different surface treatments, i.e., incorporation of chemical functional groups or molecules onto the surface. The fabrication methods of RGO and GO significantly alter their conductivity, electronic properties, and overall physicochemical properties. Unlike pure graphene, which has few or no oxygen groups, GO has oxygenated functional groups in the basal planes and sheet edges. They have a certain number of water molecules and variable oxygen-containing groups, such as hydroxyl, ether, and carboxylic acid functional groups, located between the oxidized sheets, depending on the synthetic procedure. The oxygen content is usually quite high and is typically characterized by a C/O ratio of <2.5. The reduction of GO to RGO results in a graphene-derived material that resembles pure graphene but lacks graphene's perfect crystal structure. Therefore, RGO is less hydrophilic and has a greater tendency to aggregate than GO. Researchers have reported that the tendency of the sheets to aggregate causes bacteria to settle in the aggregated regions, where they become biologically disconnected from their environment and do not multiply [66]. However, in this study, graphene in PCL/2RGO nanofiber was dispersed in the matrix without agglomeration, as previously explained in the XRD, FTIR, and FE-SEM analysis sections performed on the nanofibers. This may explain why PCL/2RGO nanofiber does not show antibacterial properties in this study.

Since the interaction of bacteria with graphene also depends on the orientation of the surface relative to the bacteria, the deposition of graphene onto the surfaces is another mechanism that significantly affects the antimicrobial character. Researchers have proposed several other mechanisms to explain the antibacterial effect of graphene,

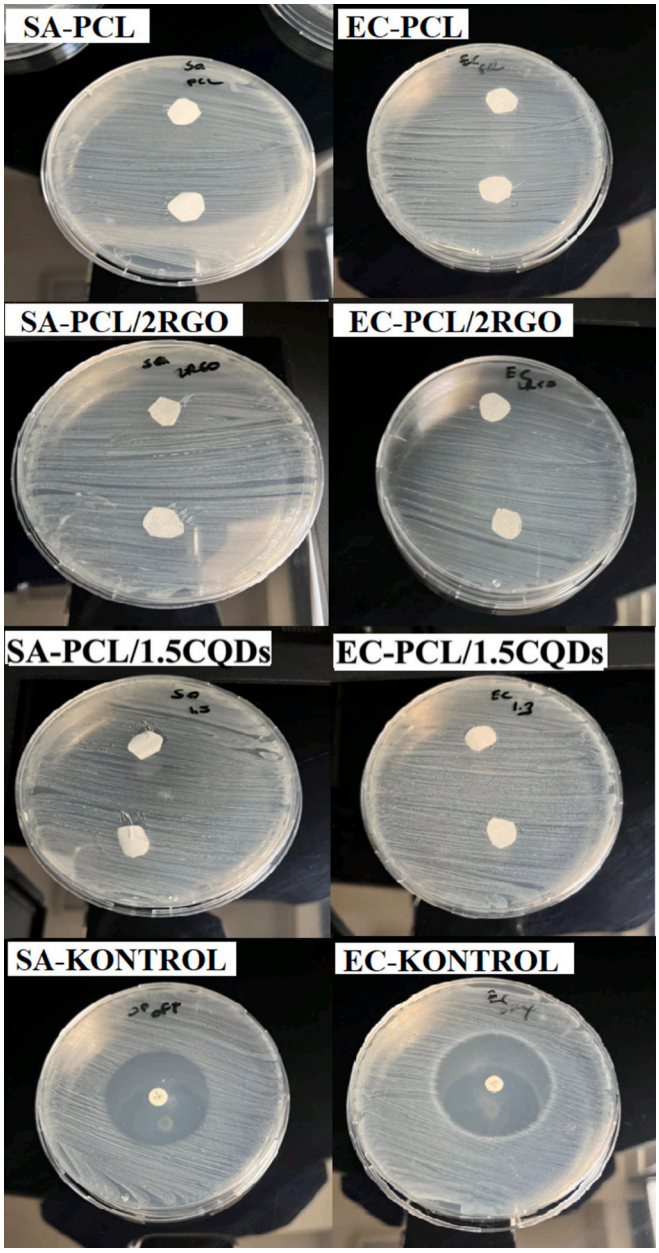

Fig. 10. Images of PCL nanofibers after antibacterial test.

including the production of reactive oxygen species, oxidative stress, or the strong extraction of large amounts of phospholipids from the bacteria's membrane. The main driving force in this mechanism is the strong Van der Waals interactions between GO nanosheets and the bacterial cell membrane. The tails of the cell membrane that are hydrophobic move into the non-oxidized hydrophobic regions of GO. On the other hand, the head groups that are hydrophilic prefer to interact with the oxygen-containing functional groups of GO through electrostatic forces. Researchers conclude that this contact's destructive lipid extraction significantly reduces cell viability and causes serious oxidative stress on the cell membrane [66]. Oxidative stress occurs when the oxidative balance is disrupted as a result of the increase in reactive oxygen species (ROS) formed by cellular metabolism with hydroxyl, superoxide, and hydrogen peroxide radicals and the inadequacy of antioxidants.

Reactive oxygen species attack the double bonds in DNA bases and lipid and protein structures in the cell, breaking off a hydrogen atom and starting chain oxidation reactions. These reactions damage macromolecules like DNA, protein, and lipid in the cell, which eventually leads to cell death [67]. The RGO sample used in this study doesn't have as many oxygen groups as GO, as reported before (RGO at.% 18.76 vs. GO at.% 46.78 [18,68]), so it doesn't interact with RGO from both the hydrophobic and hydrophilic parts of the bacterial cell membrane. This means that it can't cause a destructive extraction, doesn't produce reactive oxygen species, doesn't cause any oxidative stress, and doesn't have any antibacterial properties. Ghosal et al. reported that nanofibers produced by adding a CQDs sample from a synthetic chemical to a PCL matrix exhibited antibacterial properties [47]. Li et al. [69] determined that the antibacterial activities of CQDs produced by the hydrothermal method from a mixture of synthetic chemicals were 99.9 % and 96.54 % against *E. coli* and *S. aureus*, respectively. Saud et al. [70] reported that CQD/TiO_2 composite nanofibers exhibited antibacterial activity against *E. coli*. Nie et al. [71] investigated the antibacterial activity of CQDs samples produced from synthetic chemicals and attributed the difference in antibacterial properties observed between *E. coli* and *S. aureus* to the production of reactive oxygen species from quantum dots that damage the bacterial cell wall, leading to bacterial death. The characterization studies conducted in this study revealed that the selected PCL/1.5CQDs sample did not exhibit antibacterial properties. This was due to its lack of interaction with bacteria, unlike the RGO sample, which prevented a destructive lipid extraction from occurring. It is also thought that both RGO and CQDs doped nanofibers, which are insulators such as PCL, which do not have semiconductor properties, prevent them from having antibacterial properties. Previously, many tissue scaffold studies have reported that electrical conductivity has an important effect on the control of cell behavior [46,72]. Researchers have reported that semiconductor nanofibers with a positive surface charge demonstrate enhanced antibacterial properties [73].

4. Conclusion

The electrospinning method in this study produced nanofibers that can serve as tissue scaffolds by adding RGO and CQDs to the PCL matrix, a biodegradable polymer. The structural, thermal, mechanical, and biological properties of PCL, PCL/RGO, and PCL/CQDs nanofibers were characterized, and the results listed below were obtained.

The FTIR analysis results revealed that the interactions between the -CH_2 and C-O-C groups of PCL and the RGO and CQDs fillers were stronger than the other functional groups. The CQDs addition was the most effective filler and filler content on the crystal structure of PCL with crystal size and interlayer distance values. Both RGO and CQDs additives created a nucleation effect and increased thermal stability. The FE-SEM images of the nanofibers demonstrated that the electrospinning process successfully produced each nanofiber sample with homogeneous sizes within itself. The addition of RGO to the PCL matrix led to an increase in nanofiber diameters, while the addition of CQDs resulted in a decrease. In the conductivity test performed to explain the nanofibers were insulating properties.

The PCL/1.5CQDs nanofiber had the highest elastic modulus and nanohardness increases at 73 % and 160 %, respectively, compared to the pure PCL nanofiber. In the nanofiber samples containing RGO, a 1.9 % increase in the elastic modulus values and a 40 % increase in the nanohardness value were detected in the PCL/2RGO nanofiber. It was determined that PCL/2CQDs nanofiber, which has the highest storage and loss modulus values, increased the storage modulus by 210.79 % and the loss modulus by 595.27 % compared to pure PCL.

Biodegradability test results in PBS solution determined that nanofibers containing CQDs with lower contact angles (72.29°- 68.75°) degraded more than nanofibers containing RGO (74.96°-70.15°). The highest weight losses were determined as 3.66 % and 3.75 % in nanofiber samples containing 2.0 wt% RGO and CQDs, respectively, at the end of 56 days. The bioactivity test revealed that all nanofibers, including PCL, formed hydroxyapatite. The lack of antibacterial properties in the produced nanofibers is attributed to the fact that they do not induce oxidative stress and are insulating in nature.

CRediT authorship contribution statement

Ferda Mindivan: Writing – review & editing, Writing – original draft, Resources, Project administration, Methodology, Investigation, Formal analysis. **Büşra Boz:** Visualization, Investigation, Formal analysis.

Declaration of competing interest

The authors declare that they have no known competing financial interests or personal relationships that could have appeared to influence the work reported in this paper.

Acknowledgments

The authors declared that this study has received financial support of the research foundation (Project no: 2023-01.BŞEÜ.01-04) of Bilecik Şeyh Edebali University.

Data availability

Data will be made available on request.

References

[1] F.D. Al-Shalawi, M.A. Hanim, M.K.A. Ariffin, C.L.S. Kim, D. Brabazon, R. Calin, M. O. Al-Osaimi, Biodegradable synthetic polymer in orthopaedic application: a review, Mater. Today 74 (2023) 540–546.
[2] E. Correa, M.E. Moncada, O.D. Gutiérrez, C.A. Vargas, V.H. Zapata, Characterization of polycaprolactone/rGO nanocomposite scaffolds obtained by electrospinning, Mater. Sci. Eng. C 103 (2019) 109773.
[3] B. Joseph, A.J. John, J. Glamočlija, D. Stojković, M. Soković, S. Lazović, J. Kochupurackal, N. Kalarikkal, S. Thomas, Processing and evaluation of the structure-properties of electrospun PCL/zirconium nanoparticle scaffolds, Mater. Today Commun. 34 (2023) 104961.
[4] J.W. Kim, S. Park, K. Park, B.K. Kim, Non-toxic natural additives to improve the electrical conductivity and viscosity of polycaprolactone for melt electrospinning, Appl. Sci. 13 (3) (2023) 1844.
[5] M. Ghorghi, M. Rafienia, V. Nasirian, F.S. Bitaraf, A.M. Gharravi, A. Zarrabi, Electrospun captopril-loaded PCL-carbon quantum dots nanocomposite scaffold: fabrication, characterization, and in vitro studies, Polym. Adv. Technol. 31 (12) (2020) 3302–3315.
[6] S. Gautam, A.K. Dinda, N.C. Mishra, Fabrication and characterization of PCL/gelatin composite nanofibrous scaffold for tissue engineering applications by electrospinning method, Mater. Sci. Eng. C 33 (3) (2013) 1228–1235.
[7] S. Faraji, N. Nowroozi, A. Nouralishahi, J.S. Shayeh, Electrospun polycaprolactone/graphene oxide/quercetin nanofibrous scaffold for wound dressing: evaluation of biological and structural properties, Life Sci. 257 (2020) 118062.
[8] A. Aidun, A. Safaei Firoozabady, M. Moharrami, A. Ahmadi, N. Haghighipour, S. Bonakdar, S. Faghihi, Graphene oxide incorporated polycaprolactone/chitosan/collagen electrospun scaffold: enhanced osteogenic properties for bone tissue engineering, Artif. Organs 43 (10) (2019) E264–E281.
[9] W. Ishwarchand, G. Sarakar, B.P. Swain, Investigation of optical properties, chemical network and electronic environments of polycaprolactone/reduced graphene oxide fiber nanocomposites, Polym. Bull. 1-17 (2021).
[10] K. Kumar, A. Kumar, S. Devi, S. Tyagi, D. Kaur, Relevant photovoltaic effect in N-doped CQDs/MoS2 (0D/2D) quantum dimensional heterostructure, Ceram. Int. 48 (10) (2022) 14107–14116.
[11] P. Zhao, X. Song, M. Dong, H. Sun, W. Wu, R. Zhang, X. Zhao, Preparation and characterization of CQDs/SBS composites and its application performance as asphalt modifier, Constr. Build. Mater. 320 (2022) 126312.
[12] P.H.M. Gohari, M.H. Nazarpak, M. Solati-Hashjin, The effect of adding reduced graphene oxide to electrospun polycaprolactone scaffolds on MG-63 cells activity, Mater. Today Commun. 27 (2021) 102287.
[13] S.S. Karapehlivan, M.N. Danisik, Z. Akdag, E.N. Yildiz, O.V. Okoro, L. Nie, O. Gunduz, Fabrication and in vitro characterization of polycaprolactone/graphene oxide/collagen nanofibers for myocardial repair, Macromol. Mater. Eng. 309 (1) (2024) 2300189.
[14] C. Loyo, A. Cordoba, H. Palza, D. Canales, F. Melo, J.F. Vivanco, P.A. Zapata, Effect of gelatin coating and GO incorporation on the properties and degradability of electrospun PCL scaffolds for bone tissue regeneration, Polymers 16 (1) (2023) 129.
[15] S. Rastegar, M. Mehdikhani, A. Bigham, E. Poorazizi, M. Rafienia, Poly glycerol sebacate/polycaprolactone/carbon quantum dots fibrous scaffold as a multifunctional platform for cardiac tissue engineering, Mater. Chem. Phys. 266 (2021) 124543.
[16] M. Heidari, H. Bahrami, M. Ranjbar-Mohammadi, Fabrication, optimization and characterization of electrospun poly (caprolactone)/gelatin/graphene nanofibrous mats, Mater. Sci. Eng. C 78 (2017) 218–229.
[17] E. Ceretti, P.S. Ginestra, M. Ghazinejad, A. Fiorentino, M. Madou, Electrospinning and characterization of polymer–graphene powder scaffolds, CIRP Ann. 66 (1) (2017) 233–236.
[18] F. Mindivan, M. Göktaş, Rosehip-extract-assisted green synthesis and characterization of reduced graphene oxide, ChemistrySelect 5 (29) (2020) 8980–8985.
[19] F. Mindivan, M. Göktaş, The green synthesis of carbon quantum dots (CQDs) and characterization of polycaprolactone (PCL/CQDs) films, Colloids Surf. A Physicochem. Eng. Asp. 677 (2023) 132446.
[20] L. Xu, Y. Li, S. Gao, Y. Niu, H. Liu, C. Mei, C. Xu, Preparation and properties of cyanobacteria-based carbon quantum dots/polyvinyl alcohol/nanocellulose composite, Polymers 12 (5) (2020) 1143.
[21] M. Hashemi, A. Rostami, I. Ghasemi, A. Omrani, Incorporation of modified graphene nanoplatelets for development of bio-based shape memory polymer of polypropylene carbonate (PPC)/Polycaprolactone (PCL), J. Polym. Environ. 31 (6) (2023) 2715–2726.
[22] J.R. Dias, A. Sousa, A. Augusto, P.J. Bártolo, P.L. Granja, Electrospun polycaprolactone (PCL) degradation: an in vitro and in vivo study, Polymers 14 (16) (2022) 3397.
[23] T. Kokubo, H. Takadama, How useful is SBF in predicting in vivo bone bioactivity? Biomater 27 (15) (2006) 2907–2915.
[24] H.S. Yu, J.H. Jang, T.I. Kim, H.H. Lee, H.W. Kim, Apatite-mineralized polycaprolactone nanofibrous web as a bone tissue regeneration substrate, J. Biomed. Mater. Res. 88 (3) (2009) 747–754.
[25] W.I. Singh, S. Sinha, N.A. Devi, S. Nongthombam, S. Laha, B.P. Swain, Fabrication and characterization of reduced graphene oxide/polyaniline/poly (caprolactone) electrospun nanofiber, Arab. J. Sci. Eng. 47 (1) (2022) 925–934.
[26] J.J.P. Barros, I.D. dos Santos Silva, N.G. Jaques, M.V.L. Fook, R.M.R. Wellen, Influence of PCL on the epoxy workability, insights from thermal and spectroscopic analyses, Polym. Test. 89 (2020) 106679.
[27] T. Elzein, M. Nasser-Eddine, C. Delaite, S. Bistac, P. Dumas, FTIR study of polycaprolactone chain organization at interfaces, J. Colloid Interface Sci. 273 (2) (2004) 381–387.
[28] F. Rostami, E. Tamjid, M. Behmanesh, Drug-eluting PCL/graphene oxide nanocomposite scaffolds for enhanced osteogenic differentiation of mesenchymal stem cells, Mater. Sci. Eng. C 115 (2020) 111102.
[29] A. Marrella, G. Tedeschi, P. Giannoni, A. Lagazzo, F. Sbrana, F. Barberis, S. Scaglione, "Green-reduced" graphene oxide induces in vitro an enhanced biomimetic mineralization of polycaprolactone electrospun meshes, Mater. Sci. Eng. C 93 (2018) 1044–1053.
[30] C. Wan, B. Chen, Poly (ε-caprolactone)/graphene oxide biocomposites: mechanical properties and bioactivity, Biomed. Mater. 6 (5) (2011) 055010.
[31] A.B. Pebdeni, M. Hosseini, A. Barkhordari, Smart fluorescence aptasensor using nanofiber functionalized with carbon quantum dot for specific detection of pathogenic bacteria in the wound, Talanta 246 (2022) 123454.
[32] G. El Fawal, H. Hong, X. Mo, H. Wang, Fabrication of scaffold based on gelatin and polycaprolactone (PCL) for wound dressing application, J. Drug Deliv. Technol. 63 (2021) 102501.
[33] M. Bagheri, A. Mahmoodzadeh, Polycaprolactone/graphene nanocomposites: synthesis, characterization and mechanical properties of electrospun nanofibers, J. Inorg. Organomet. Polym. Mater. 30 (5) (2020) 1566–1577.
[34] V. Kheiri Mollaqasem, A. Asefnejad, M.R. Nourani, V. Goodarzi, M.R. Kalaee, Incorporation of graphene oxide and calcium phosphate in the PCL/PHBV core-shell nanofibers as bone tissue scaffold, J. Appl. Polym. Sci. 138 (6) (2021) 49797.
[35] A. Fakhrali, M. Nasari, N. Poursharifi, D. Semnani, H. Salehi, M. Ghane, S. Mohammadi, Biocompatible graphene-embedded PCL/PGS-based nanofibrous scaffolds: a potential application for cardiac tissue regeneration, J. Appl. Polym. Sci. 138 (40) (2021) 51177.
[36] S. Gungordu Er, T.A. Tabish, M. Edirisinghe, R.K. Matharu, Antiviral properties of porous graphene, graphene oxide and graphene foam ultrafine fibers against Phi6 bacteriophage, Front. Med. 9 (2022) 1032899.
[37] R.S. Rajaura, S. Srivastava, V. Sharma, P.K. Sharma, C. Lal, M. Singh, Y.K. Vijay, Role of interlayer spacing and functional group on the hydrogen storage properties of graphene oxide and reduced graphene oxide, Int. J. Hydrog. Energy 41 (22) (2016) 9454–9461.
[38] M. Mohseni, P. Toloee, N. Nademi, Rheological and electrical behavior of core–shell conduit comprising PCL-chitosan-gelatin/Al_2O_3 nanofibers and gellan-agar/polyaniline-graphene, J. Macromol. Sci. A 59 (12) (2022) 818–827.
[39] P. Sehrawat, S. Parveen, S.A. Hashmi, High-performance sodium ion conducting gel polymer electrolyte based on a biodegradable polymer polycaprolactone, Energy Storage 5 (2) (2023) e375.
[40] H.Y. Mi, X. Jing, J. Peng, M.R. Salick, X.F. Peng, L.S. Turng, Poly (ε- caprolactone) (PCL)/cellulose nano-crystal (CNC) nanocomposites and foams, Cellulose 21 (2014) 2727–2741.
[41] M.A. Taghavi, S.M. Rabiee, M. Jahanshahi, F. Nasiri, Electrospun poly-ε-caprolactone (PCL)/dicalcium phosphate dihydrate (DCPD) composite scaffold for tissue engineering application, Mol. Biotechnol. 61 (2019) 345–354.
[42] A.P. Golin, Humidity Effect on the Structure of Electrospun Core-Shell PCL-PEG Fibers for Tissue Regeneration Applications, MSc thesis, The University of Western Ontario, Canada, 2014.
[43] S. Behtaj, F. Karamali, E. Masaeli, Y.G. Anissimov, M. Rybachuk, Electrospun PGS/PCL, PLLA/PCL, PLGA/PCL and pure PCL scaffolds for retinal progenitor cell cultivation, Biochem. Eng. J. 166 (2021) 107846.

[44] A. Sadeghi, F. Moztarzadeh, J.A. Mohandesi, Investigating the effect of chitosan on hydrophilicity and bioactivity of conductive electrospun composite scaffold for neural tissue engineering, Int. J. Biol. Macromol. 121 (2019) 625–632.
[45] M. Shabankhah, A. Moghaddaszadeh, N. Najmoddin, 3D printed conductive PCL/GO scaffold immobilized with gelatin/CuO accelerates H9C2 cells attachment and proliferation, Prog. Org. Coat. 186 (2024) 108013.
[46] M. Jaymand, R. Sarvari, P. Abbaszadeh, B. Massoumi, M. Eskandani, Y. Beygi-Khosrowshahi, Development of novel electrically conductive scaffold based on hyperbranched polyester and polythiophene for tissue engineering applications, J. Biomed. Mater. Res. A 104 (11) (2016) 2673–2684.
[47] K. Ghosal, M. Kováčová, P. Humpolíček, J. Vajďák, M. Bodík, Z. Špitalský, Antibacterial photodynamic activity of hydrophobic carbon quantum dots and polycaprolactone based nanocomposite processed via both electrospinning and solvent casting method, Photodiagn. Photodyn. Ther. 35 (2021) 102455.
[48] P. Tyagi, S.A. Catledge, A. Stanishevsky, V. Thomas, Y.K. Vohra, Nanomechanical properties of electrospun composite scaffolds based on polycaprolactone and hydroxyapatite, J. Nanosci. Nanotechnol. 9 (8) (2009) 4839–4845.
[49] A. Gloria, B. Frydman, M.L. Lamas, A.C. Serra, M. Martorelli, J.F. Coelho, M. Domingos, The influence of poly (ester amide) on the structural and functional features of 3D additive manufactured poly (ε-caprolactone) scaffolds, Mater. Sci. Eng. C 98 (2019) 994–1004.
[50] V. Thomas, M.V. Jose, S. Chowdhury, J.F. Sullivan, D.R. Dean, Y.K. Vohra, Mechano-morphological studies of aligned nanofibrous scaffolds of polycaprolactone fabricated by electrospinning, J. Biomater. Sci. Polym. Ed. 17 (9) (2006) 969–984.
[51] M. Petretta, A. Gambardella, M. Boi, M. Berni, C. Cavallo, G. Marchiori, V. Cannillo, Composite scaffolds for bone tissue regeneration based on PCL and Mgcontaining bioactive glasses, Biology 10 (5) (2021) 398.
[52] S. Salehi, T. Bahners, J.S. Gutmann, S.L. Gao, E. Mäder, T.A. Fuchsluger, Characterization of structural, mechanical and nano-mechanical properties of electrospun PGS/PCL fibers, RSC Adv. 4 (33) (2014) 16951–16957.
[53] H. Yan, G. Tian, K. Sun, Y. Zhang, Y. Zhang, Effect of silane coupling agent on the polymer-filler interaction and mechanical properties of silica-filled NR, J. Polym. Sci., Part B: Polym. Phys. 43 (5) (2005) 573–584.
[54] A. Sonseca, L. Peponi, O. Sahuquillo, J.M. Kenny, E. Giménez, Electrospinning of biodegradable polylactide/hydroxyapatite nanofibers: study on the morphology, crystallinity structure and thermal stability, Polym. Degrad. Stab. 97 (10) (2012) 2052–2059.
[55] A.N. Frone, D.M. Panaitescu, I. Chiulan, A.R. Gabor, C.A. Nicolae, M. Oprea, A. C. Puitel, Thermal and mechanical behavior of biodegradable polyester films containing cellulose nanofibers, J. Therm. Anal. Calorim. 138 (2019) 2387–2398.
[56] I.E. Uflyand, E.G. Drogan, V.E. Burlakova, K.A. Kydralieva, I.N. Shershneva, G. I. Dzhardimalieva, Testing the mechanical and tribological properties of new metal-polymer nanocomposite materials based on linear low-density polyethylene and Al65Cu22Fe13 quasicrystals, Polym. Test. 74 (2019) 178–186.
[57] F. Mindivan, M. Göktaş, A.S. Dike, Mechanical, thermal, and micro-and nanostructural properties of polyvinyl chloride/graphene nanoplatelets nanocomposites, Polym. Compos. 41 (9) (2020) 3707–3716.
[58] C.L. Salgado, E.M. Sanchez, C.A. Zavaglia, P.L. Granja, Biocompatibility and biodegradation of polycaprolactone-sebacic acid blended gels, J. Biomed. Mater. Res. A 100 (1) (2012) 243–251.
[59] C. Srinivasa Reddy, J. Reddy Venugopal, S. Ramakrishna, E. Zussman, Polycaprolactone/oligomer compound scaffolds for cardiac tissue engineering, J. Biomed. Mater. Res. A 102 (10) (2014) 3713–3725.
[60] V.N. Malheiro, S.G. Caridade, N.M. Alves, J.F. Mano, New poly (ε- caprolactone)/chitosan blend fibers for tissue engineering applications, Acta Biomater. 6 (2) (2010) 418–428.
[61] X. Luo, P.T. Mather, Preparation and characterization of shape memory elastomeric composites, Macromolecules 42 (19) (2009) 7251–7253.
[62] M. Gümüşderelioğlu, F.B. Kaya, I.G. Beşkardeş, Comparison of epithelial and fibroblastic cell behavior on nano/micro-topographic PCL membranes produced by crystallinity control, J. Colloid Interface Sci. 358 (2) (2011) 444–453.
[63] S. Afza, H. Esfahani, A. Nourian, M.R. Ghaani, A novel approach to biomineralization of electrospun PCL scaffolds by protein and hydroxyapatite nanoparticles; molecular dynamics simulation and in-vitro evaluation, Eur. Polym. J. 182 (2023) 111739.
[64] A. Radisavljevic, D.B. Stojanovic, S. Perisic, V. Djokic, V. Radojevic, M. Rajilic-Stojanovic, P.S. Uskokovic, Cefazolin-loaded polycaprolactone fibers produced via different electrospinning methods: characterization, drug release and antibacterial effect, Eur. J. Pharm. Sci. 124 (2018) 26–36.
[65] S. Sivakumar, V. Sadaiyandi, S. Swaminathan, R. Ramalingam, Biocompatibility, anti-hemolytic, and antibacterial assessments of electrospun PCL/collagen composite nanofibers loaded with Acanthophora spicifera extracts mediated copper oxide nanoparticles, Biocatal. Agric. Biotechnol. 55 (2024) 102983.
[66] S. Szunerits, R. Boukherroub, Antibacterial activity of graphene-based materials, J. Mater. Chem. B 4 (43) (2016) 6892–6912.
[67] O. Özcan, H. Erdal, G. Çakırca, Z. Yönden, Oksidatif stres ve hücre içi lipit, protein ve DNA yapıları üzerine etkileri, J. Clin. Exp. Investig. 6 (3) (2015) 331–336.
[68] F. Mindivan, M. Göktaş, Preparation of new PVC composite using green reduced graphene oxide and its effects in thermal and mechanical properties, Polym. Bull. 77 (4) (2020) 1929–1949.
[69] Z. Li, J. Ai, D. Wu, Y. Yu, L. Xie, H. Ke, Q. Wei, Robust integration of light-driven carbon quantum dots with bacterial cellulose enables excellent mechanical and antibacterial biodegradable yarn, Int. J. Biol. Macromol. 257 (2024) 128741.
[70] P.S. Saud, B. Pant, A.M. Alam, Z.K. Ghouri, M. Park, H.Y. Kim, Carbon quantum dots anchored TiO_2 nanofibers: effective photocatalyst for waste water treatment, Ceram. Int. 41 (9) (2015) 11953–11959.
[71] X. Nie, S. Wu, A. Mensah, K. Lu, Q. Wei, Carbon quantum dots embedded electrospun nanofibers for efficient antibacterial photodynamic inactivation, Mater. Sci. Eng. C 108 (2020) 110377.
[72] H.L. Nguyen, Y.K. Jo, M. Cha, Y.J. Cha, D.K. Yoon, N.D. Sanandiya, D.S. Hwang, Mussel-inspired anisotropic nanocellulose and silver nanoparticle composite with improved mechanical properties, electrical conductivity and antibacterial activity, Polymers 8 (3) (2016) 102.
[73] S. Bhattacharya, D. Kim, S. Gopal, A. Tice, K. Lang, J.S. Dordick, R.J. Linhardt, Antimicrobial effects of positively charged, conductive electrospun polymer fibers, Mater. Sci. Eng. C 116 (2020) 111247.